Bioactive Materials 25 (2023) 657–676

Contents lists available at ScienceDirect

Bioactive Materials

journal homepage: www.keaipublishing.com/en/journals/bioactive-materials

Step-wise CAG@PLys@PDA-Cu^{2+} modification on micropatterned nanofibers for programmed endothelial healing

Bingcheng Yi [a,b,1], Boya Zhou [a,1], Zhenfeng Song [a], Lei Yu [a], Wenbo Wang [a,**], Wei Liu [a,*]

[a] Department of Plastic and Reconstructive Surgery, Shanghai Key Laboratory of Tissue Engineering, Shanghai Ninth People's Hospital, Shanghai Jiao Tong University School of Medicine, Shanghai, 200011, China
[b] Department of Vascular Surgery, Shanghai Ninth People's Hospital, Shanghai Jiao Tong University School of Medicine, Shanghai, 200011, China

ARTICLE INFO

Keywords:
Surface chemistry
Anisotropic topography
Step-wise modification
Endothelial healing
Functional vascular grafts

ABSTRACT

Native-like endothelium regeneration is a prerequisite for material-guided small-diameter vascular regeneration. In this study, a novel strategy is proposed to achieve phase-adjusted endothelial healing by step-wise modification of parallel-microgroove-patterned (i.e., micropatterned) nanofibers with polydopamine-copper ion (PDA-Cu^{2+}) complexes, polylysine (PLys) molecules, and Cys-Ala-Gly (CAG) peptides (CAG@PLys@PDA-Cu^{2+}). Using electrospun poly(L-lactide-*co*-caprolactone) random nanofibers as the demonstrating biomaterial, step-wise modification of CAG@PLys@PDA-Cu^{2+} significantly enhanced substrate wettability and protein adsorption, exhibited an excellent antithrombotic surface and outstanding phase-adjusted capacity of endothelium regeneration involving cell adhesion, endothelial monolayer formation, and the regenerated endothelium maturation. Upon *in vivo* implantation for segmental replacement of rabbit carotid arteries, CAG@PLys@PDA-Cu^{2+} modified grafts (2 mm inner diameter) with micropatterns on inner surface effectively accelerated native-like endothelium regeneration within 1 week, with less platelet aggregates and inflammatory response compared to those on non-modified grafts. Prolonged observations at 6- and 12-weeks post-implantation demonstrated a positive vascular remodeling with almost fully covered endothelium and mature smooth muscle layer in the modified vascular grafts, accompanied with well-organized extracellular matrix. By contrast, non-modified vascular grafts induced a disorganized tissue formation with a high risk of thrombogenesis. In summary, step-wise modification of CAG@PLys@PDA-Cu^{2+} on micropatterned nanofibers can significantly promote endothelial healing without inflicting thrombosis, thus confirming a novel strategy for developing functional vascular grafts or other blood-contacting materials/devices.

1. Introduction

Endothelium plays a critical role in maintaining vascular homeostasis [1]. Dysfunctional endothelium is implicated in various diseases including thrombosis and intimal hyperplasia, which is the leading cause of mortality worldwide [2]. Recently, biomimicking vascular graft is considered as a promising alternative to the repair of diseased vessels, especially for the small-diameter blood vessels ($\varphi < 4$ mm) [3]. To accelerate endothelialization, various functional modifications such as native-like topographical, biochemical and mechanical cues have been applied to the preparation of related vascular grafts [4,5]. Nevertheless, endothelium regeneration remains far from ideal, which ultimately results in dramatical occlusion of implanted grafts [6] due to the limited biological functions of vascular grafts, as the current-used strategies are only able to partially regulate EC behaviors. Actually, material-guided *in situ* endothelial healing involves diverse biological events, including recruitment and adhesion of host endothelial cells/endothelial progenitor cells (ECs/EPCs), cell spreading and compact endothelial monolayer formation, and endothelial monolayer maturation [5,7,8], which constitute a continuous and complicated remodeling process. Therefore,

Peer review under responsibility of KeAi Communications Co., Ltd.
* Corresponding author. Department of Plastic and Reconstructive Surgery, Shanghai Key Laboratory of Tissue Engineering, Shanghai Ninth People's Hospital, Shanghai Jiao Tong University School of Medicine, 639 Zhi Zao Ju Road, Shanghai, 200011, China.
** Corresponding author. Department of Plastic and Reconstructive Surgery, Shanghai Key Laboratory of Tissue Engineering, Shanghai Ninth People's Hospital, Shanghai Jiao Tong University School of Medicine, 639 Zhi Zao Ju Road, Shanghai, 200011, China.
E-mail addresses: wangwenbo0903@126.com (W. Wang), liuwei_2000@yahoo.com (W. Liu).
[1] These authors contributed equally to this study.

https://doi.org/10.1016/j.bioactmat.2022.07.010
Received 9 May 2022; Received in revised form 23 June 2022; Accepted 8 July 2022
Available online 14 July 2022

developing a novel strategy to achieve phase-adjusted endothelial healing on vascular grafts is necessary. Unfortunately, such concept has always been ignored.

Host cell recruitment is the first essential biological event in endothelial healing [9]. To date, numerous studies have focused on the immobilization of bioactive molecules (e.g., extracellular matrix (ECM) proteins [5] and ECM polysaccharides [10,11]) onto vascular grafts to facilitate EC recruitment, adhesion and ingrowth. But, most of the molecules may also stimulate platelet adhesion and smooth muscle cell (SMC) growth, which inflicts a high risk of thrombosis and intimal hyperplasia [5]. Since ECM components have been recognized to delineate specific tissue locations with cell-selective ability, EC-selective peptides such as Arg-Glu-Asp-Val (REDV) derived from fibronectin [12], Tyr-Lle-Gly-Ser-Arg (YIGSR) from laminin [13], and Cys-Ala-Gly (CAG) from collagen IV [14] have been developed and widely utilized to promote EC adhesion. Among them, CAG-peptides exhibit an outstanding inhibitory effect on SMC adhesion [15] and incapability of interacting with circulated blood cells and platelets [16,17]. Therefore, modification with CAG peptides on vascular grafts may provide an effective strategy to promote selective cell adhesion for the initial stage of material-guided *in situ* endothelialization.

After EC recruitment and adhesion on graft surface, cell-substrate interaction plays a critical role in the subsequent EC spreading and endothelial monolayer formation [18]. Given that the effect of substrate topography and stiffness is more potent than that of surface chemistry on directing cell behavior [19,20], electrospun nanofibers are of great interest in engineering vascular grafts, because of their biomimetic nanofeature and sufficient softness that benefit cell-matrix interaction [21], especially for the aligned nanofibers that promote native-like endothelial formation with oriented morphology [22,23]. However, the apparent shortcomings of fiber structural instability upon shear flows, dense fiber accumulation, and inherent anisotropic mechanical properties as well limit the potential of aligned nanofibers for their clinical applications [24]. Recently, creating parallel microgrooves on random nanofibrous substrates (micropatterned nanofibers) has been demonstrated capable of effectively inducing orientated endothelium regeneration with native-like morphology and enhancing endothelial maturation *via* improving cell-matrix interaction [24]. This offers an effective approach for the formation of compact native-like endothelial monolayer in material-guided *in situ* endothelialization.

Complete EC monolayer formation is not synonymous with full restoration of endothelial functions [4]. After rapid endothelialization on graft surface, promoting EC functions become another prerequisite for endothelium healing. Nitric oxide (NO), continuously released by natural ECs, can regulate several crucial physiological processes in blood vessels, including anti-SMC proliferation, anti-platelet activation/aggregation, and anti-inflammation [25,26]. Thus, diversified NO-releasing-based vascular grafts have been developed, including NO-releasing approaches (immobilization of NO donor) and catalytic NO-generating approaches (utilization of NO catalyst) [27]. Unlike NO-releasing approaches with limited storage [28], catalytic NO-generating approaches can continuously and steadily generate NO in a local position from endogenous S-nitrosothiols (RSNOs) in blood, and thus become an attracting approach [29,30]. Given that the glutathione peroxidase (GPx)-like activity (catalyzing NO release from RSNOs *in situ*) of copper ions (Cu^{2+}) linked to the polydopamine (PDA) film can strongly adhere to almost any substrates [31,32], one-step metal-catecholamine assembling strategy was recently put forward to form PDA-Cu^{2+} coordination complexes on vascular graft surface [33]. More interestingly, the yielded PDA-Cu^{2+} coating not only exhibits long-term NO-catalytic activity, but also allows the secondary grafting of amide-contained bioactive molecules [34], which acts as a promising platform for improving maturation of the regenerated endothelial monolayer in material-guided *in situ* endothelialization.

Furthermore, vascular injury will activate coagulation pathways to motivate platelet adhesion/activation after graft implantation, which can also reduce the long-term effectiveness of vascular grafts. Hence, an effective antithrombotic surface is required, especially at the stage of endothelium development. Although heparin, a derivative of EC-secreted heparan sulfate, has been widely used for improving substrate antithrombogenicity, it presents the risk of bleeding and heparin-induced thrombocytopenia in clinical use [35]. As another pro-angiogenesis molecule [36], lysine (Lys) has been verified able to lyse clots *via* selectively binding plasma plasminogen and avoiding nonspecific protein adsorption [37,38], thereby exhibiting the excellent capacity of inhibiting thrombus formation. Recently, Lysmodification was confirmed to significantly improve graft antithrombogenicity in our previous work [22]. This indicates that selecting Lys-contained bioactive molecules like polylysine (PLys) to modify vascular grafts may effectively compensate for the insufficient antithrombogenicity of the scaffolds during material-guided *in situ* endothelialization. More interestingly, the abundant amine groups of PLys molecules can provide a robust anchor for CAG grafting.

Herein, poly(L-lactide-*co*-caprolactone) (PLCL) was applied as the basic biomaterial to fabricate nanofibers, because it is a common research biodegradable elastic polymer that has been widely used as a vascular substitute for small-diameter vascular regeneration [6,39,40]. Then, a novel strategy of programmed endothelial regeneration was developed by step-wise modification of the micropatterned nanofibers with PDA-Cu^{2+} complexes, PLys molecules, and CAG peptides (Fig. 1A). The yielded vascular grafts were speculated to programmatically regulate host EC capture and adhesion, accelerate oriented endothelial monolayer formation, promote regenerated endothelium maturation, and thus concurrently suppress thrombosis formation (Fig. 1B). To verify this proposed strategy, a thorough characterization was performed to examine the surface properties of the modified substrates. After that, the effects of the yielded coating layer on EC adhesion, EC monolayer integrity, EC monolayer maturation, and antithrombogenicity were assessed. Lastly, micropatterned PLCL nanofibers with the developed modification were used to construct small-diameter vascular grafts (2 mm inner diameter) and then implanted in rabbit carotid artery defect model for proof-of-concept evaluation.

2. Materials and methods

2.1. Preparation of scaffolds with the programmed regulation of EC behaviors

2.1.1. Electrospinning of PLCL nanofibers

Electrospinning was employed to fabricate random PLCL nanofibers. Briefly, polymeric solution (4%, w/v) was prepared through dissolving PLCL (LA/CL 50:50, IV 2.9 dl/g, Daigang, China) into 1,1,1,3,3,3-hexafluoro-2-propanol (HFIP, Chembee, China). After being stirring for 12 h, polymeric solution was electrospun into nanofibers as the following parameters: applied voltage 13 kV, flow rate 0.5 mL/h, needle tip to drum-collector gap distance 18 cm, and ambient conditions (20–25 °C and 25–30% humidity). Then, the produced PLCL nanofibers were subjected to vacuum-drying. To fabricate the micropatterned nanofibers, the silicon wafer (Suzhou Cchip Scientific Instrument Co. Ltd., China) with 20 μm groove width and 20 μm groove depth was fabricated using laser engraving. Then, the silicon wafer was used as the element for collecting nanofibers during electrospinning (Fig. 1A). In this study, 20 μm size of parallel microgrooves was chosen because it can effectively induce native-like endothelium with oriented morphology *via* contact guidance [24,41].

2.1.2. CAG@PLys@PDA-Cu^{2+} modification of PLCL nanofibers

Dopamine/copper chloride solution was prepared by co-dissolving dopamine (2 mg/mL, Sigma, USA) and copper chloride (0.5 mg/mL, Sinopharm Chemical Reagent, China) in Tris-HCl buffer (10 mM, pH 8.5, Shanghai Yuan Mu Biotechnology, China). PLCL nanofibers were then immersed into the prepared solution (open to the air) under gentle

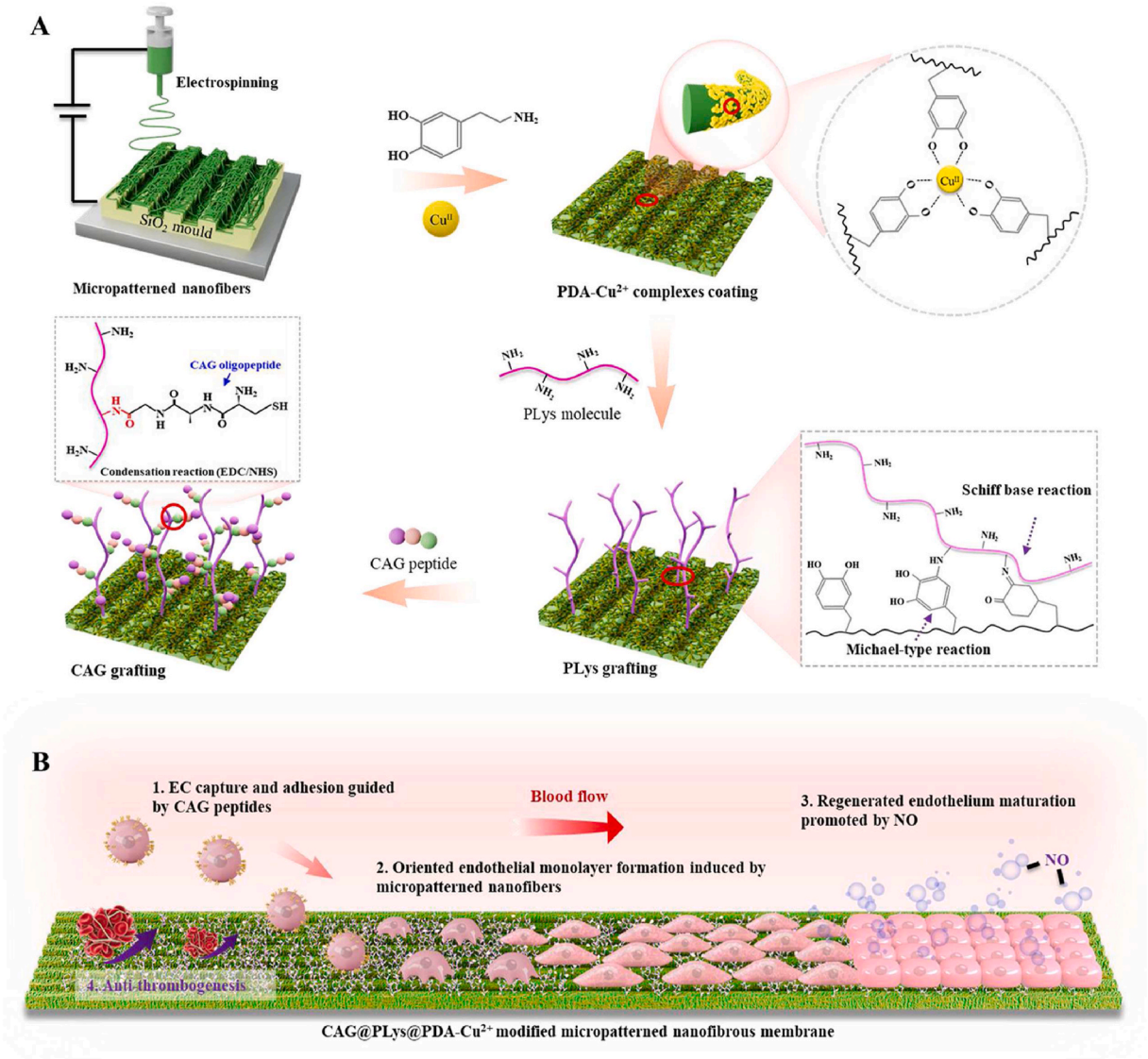

Fig. 1. Schematic of step-wise modification on vascular grafts for programmed endothelial healing: (A) Step-wise modification of micropatterned nanofibers with PDA-Cu^{2+} complexes, PLys molecules, and CAG peptides; (B) Functions of the yielded vascular grafts to phase-adjust endothelial regeneration: 1) Promoting host EC capture and adhesion; 2) Guiding the adhered ECs to form an oriented endothelial monolayer; 3) Enhancing the maturation of the regenerated endothelium; 4) Suppressing thrombogenesis.

shaking at 100 rpm for 12 h at room temperature. Afterwards, the treated nanofibers were retrieved and rinsed thoroughly with deionized water to obtain PDA-Cu^{2+} modified PLCL nanofibers (name as PLCL@PDA-Cu). Then, PLys solution (1 mg/mL, pH 8.5) was prepared by dissolving PLys (MW ~5000, Macklin, China) in Tris-HCl buffer (10 mM, pH8.5), followed by the immersion of the PDA-Cu^{2+} modified PLCL nanofibers for 12 h under gentle shaking at 100 rpm. After being rinsed thoroughly with deionized water, the PLys@PDA-Cu^{2+} modified nanofibers were obtained and named as PLCL@PDA-Cu@PLys. Finally, CAG peptides (ChinaPeptides, China) were dissolved into phosphate buffer saline (PBS) solution to prepare CAG solution (1 mg/mL), and the solution pH was adjusted to 5.5. After the addition of 1-ethyl-3-(-3-dimethylaminopropyl) carbodiimide hydrochloride (EDC, 5 mg/mL, TCI, Japan) and N-hydroxysuccinimide (NHS, 3 mg/mL, TCI, Japan) to activate the –COOH groups of CAG molecules, the PLys@PDA-Cu^{2+} modified PLCL nanofibers were immersed into the CAG solution for 2 h under gentle shaking at 100 rpm. Then, the treated nanofibers were retrieved and rinsed thoroughly with deionized water to obtain CAG@PLys@PDA-Cu^{2+} modified PLCL nanofibers (name as PLCL@PDA-Cu@PLys@CAG).

2.2. Characterization of the obtained scaffolds

2.2.1. Surface morphology

Surface morphology of the pristine PLCL nanofibers, PDA-Cu^{2+} modified, PLys@PDA-Cu^{2+} modified, and CAG@PLys@PDA-Cu^{2+} modified nanofibers was observed by a scanning electron microscope (SEM, Sigma 300, ZEISS) under an acceleration voltage of 0.02–30 kV. Prior to imaging, all samples were sputter-coated with gold for 30 s to increase substrate conductivity. To verify the successful modification, the element mapping (e.g., C, Cu, N, and S) of CAG@PLys@PDA-Cu^{2+} functionalized nanofibers was further employed by Energy Dispersive X-ray Spectrometry (EDS, Smartedx, ZEISS).

To visually observe the morphology variation of samples, the surface topography and roughness of single fiber were analyzed using a NT-MDT Prima Dimension FastScan atomic force microscope (AFM, Bruker, Germany). AFM images with scanning area of 0.5 × 0.5 μm were generated by scanning with ScanAsyst mode using a silicon nitride

probe, and the average surface roughness of single fiber was measured from the obtained AFM images *via* NanoScope Analysis software.

2.2.2. Surface chemistry

Surface elemental composition of pristine PLCL nanofibers, PDA-Cu^{2+} modified, PLys@PDA-Cu^{2+} modified, and CAG@PLys@PDA-Cu^{2+} modified nanofibers was employed *via* X-ray photoelectron spectroscopy (XPS, Thermo Scientific K-Alpha+, USA) with a monochromic Al Kα excitation source at 100 eV. The C 1s and N 1s spectra of samples were fitted with the Origin 9.0 software by Gaussian-Lorentzian function.

Fourier transform infrared (FTIR) spectroscopy of pristine PLCL nanofibers, PDA-Cu^{2+} modified, PLys@PDA-Cu^{2+} modified, and CAG@PLys@PDA-Cu^{2+} modified nanofibers were evaluated by a FTIR spectrometer (Thermo IS5, USA) over the wavenumber range of 4000–800 cm^{-1}. Data collection was carried out by accumulation of 32 scans with a resolution of 4 cm^{-1}.

2.2.3. Surface wettability, tensile property and zeta potential

Surface wettability of pristine PLCL nanofibers, PDA-Cu^{2+} modified, PLys@PDA-Cu^{2+} modified, and CAG@PLys@PDA-Cu^{2+} modified nanofibers was examined by measuring the water contact angle (WCA) with an optical tensiometer (Dataphysics DCAT20, Germany). Briefly, 2 μL deionized water was used as the probe liquid to drop onto each fibrous membrane, and then the droplet was photographed to get the WCA images.

Tensile properties of pristine PLCL nanofibers, PDA-Cu^{2+} modified, PLys@PDA-Cu^{2+} modified, and CAG@PLys@PDA-Cu^{2+} modified nanofibers (3 cm × 2 cm) in wet state were detected on a tabletop tensile tester (Instron, USA) at a stretching speed of 10 mm/min. Prior to testing, all samples were immersed in deionized water for 24 h. Then, tensile strength and Young's modulus were derived from the generated stress-strain curves.

Zeta potential of pristine PLCL nanofibers, PDA-Cu^{2+} modified, PLys@PDA-Cu^{2+} modified, and CAG@PLys@PDA-Cu^{2+} modified nanofibers was determined using streaming potential at pH 4, 7 and 10 *via* a SurPASS 3 Electrokinetic Analyzer (Anton Paar GmbH, Austria), in which potassium chloride solution (1 mM) was chosen as the background electrolyte solution for testing at room temperature.

2.2.4. Surface protein adsorption capacity

Surface protein adsorption capacity of pristine PLCL nanofibers, PDA-Cu^{2+} modified, PLys@PDA-Cu^{2+} modified, and CAG@PLys@PDA-Cu^{2+} modified nanofibers was evaluated using bicinchoninic acid (BCA) protein assay kit (Solarbio, China). Briefly, circular-shaped fibrous membranes (15 mm diameter) were placed in 24-well plates and then incubated with 200 μL of bovine serum albumin (BSA, 50 μg/mL, Sangon Biotech, China) solution for 2 h at room temperature. Afterwards, the treated fibrous membranes were rinsed thoroughly with deionized water 3 times and then incubated with 300 μL of BCA reagent for 30 min at 37 °C. Lastly, to analyze the content of the adsorbed BSA, 100 μL of the solution was transferred into a 96-well plate and the absorbance at 562 nm was measured with a microplate reader (Thermo, USA).

To visually observe the adsorbed BSA on samples, the circular fibrous membranes were also placed in 24-well plates and then incubated with 200 μL of fluorescein isothiocyanate labeled BSA (FITC-BSA, 50 μg/mL, Sangon Biotech, China) solution for 2 h in the dark. After being rinsed thoroughly with deionized water, the treated samples were observed under a laser-scanning confocal microscopy (Carl Zeiss, Germany).

2.3. Capacity verification of the developed CAG@PLys@PDA-Cu^{2+} coating for EC capture

2.3.1. Cell culture and seeding

Human umbilical vein endothelial cells (huvECs, ScienCell, USA) were cultured in a complete medium, namely, human Endothelial Cell Medium (hECM, ScienCell, USA) that contains 5% fetal bovine serum (FBS), 1% penicillin/streptomycin and 1% endothelial cell growth factor supplements, with the culture medium changed every 2 days. For cell seeding, the samples were sterilized by ultraviolet light irradiation for 6 h, followed by the treatment of 75% ethanol for 2 h. After being washed 3 times with PBS, the sterilized samples were placed in 24-well culture plates and then pre-incubated with hECM overnight at 37 °C. Finally, the cultured huvECs (3–8 passages) with 90% confluence were collected using trypsin-EDTA, and then seeded onto the treated samples.

2.3.2. Cell adhesion and spreading

To indirectly assess the capacity of scaffolds for capturing ECs, huvEC adhesion and their spreading were performed by seeding cells onto the fibrous samples at a density of 3×10^4 cells/cm^2. After culture of the cell-scaffold constructs for 10 min and 2 h respectively, actin cytoskeleton and cell nucleus of the adhered huvECs were stained with phalloidin and 4',6-diamidino-2-phenylindole (DAPI) to evaluate cell adhesion and cell spreading. Briefly, the cell-seeded constructs were fixed in 4% paraformaldehyde (Biosharp, China) for 30 min, followed by the permeation with 0.2% Triton X-100 (Solarbio, China) for 5 min. After being rinsed thoroughly with PBS, the actin cytoskeleton of huvECs was stained with TRITC Phalloidin (1:200 dilution, Yeasen Biotechnology, China) for 30 min and the cell nuclei was stained with DAPI (1:1000 dilution, Yeasen Biotechnology, China) for 10 min at room temperature in the dark. Then, observations of cell adhesion and spreading were respectively conducted using the laser-scanning confocal microscopy. Based on the obtained fluorescence images, the adhered cell number in square millimeter and average cell area of cell spreading were analyzed *via* ImageJ software.

2.3.3. Focal adhesion formation

Focal adhesion (FA) formation of huvECs was further observed to analyze cell-matrix interaction using immunofluorescence staining of integrin β1. huvECs were seeded onto the fibrous samples at a density of 3×10^4 cells/cm^2 in 24-well culture plates. After culture for 3 days, the integrin β1 expression in single huvECs was analyzed using immunofluorescent staining. Briefly, the cell-seeded constructs were fixed in 4% paraformaldehyde for 30 min and permeabilized with 0.2% Triton X-100 for 5 min. After being blocked by 10% goat serum (Solarbio, China) for 30 min, the constructs were incubated with rabbit anti-human integrin β1 polyclonal antibody (1:200 dilution, Proteintech, USA) overnight at 4 °C, followed by the incubation of fluorescein (FITC)-conjugated affinipure goat anti-rabbit IgG (H+L) antibody (1:50 dilution, Proteintech, USA) for 90 min at room temperature. Then, cell nuclei of huvECs were counterstained with DAPI for 10 min, and the integrin β1 expression of single huvECs was observed under laser-scanning confocal microscopy. For quantitative analysis of FA size distribution and FA number per cell, integrin β1 analysis of the obtained images was performed by a Focal Adhesion Analysis Server [42,43].

2.4. Capacity verification of the developed CAG@PLys@PDA-Cu^{2+} coating for inducing compact endothelial monolayer formation

2.4.1. huvEC monolayer morphology and integrity

huvECs were seeded onto the fibrous samples at a high density of 3×10^5 cells/cm^2 in 24-well plates to allow the formation of confluent cell monolayer. After culture for 3 days, huvEC monolayer morphology was observed by fluorescence staining of actin cytoskeleton with phalloidin and cell nucleus counterstaining with DAPI. The detailed process was conducted following the protocol in **Section 2.3.2**. Then, observation of the regenerated huvEC monolayer was conducted using laser-scanning confocal microscopy. For huvEC monolayer integrity, immunofluorescent staining of VE-cadherin (a cell-cell junction marker [23]) was performed with rabbit anti-human VE-cadherin antibody (1:200 dilution, Bioss, China) as the primary antibody and FITC-conjugated affinipure goat anti-rabbit IgG (H+L) (1:50 dilution) as the secondary antibody. The detailed process was conducted following the protocol in

Section 2.3.3. Afterwards, the constructs were observed under laser-scanning confocal microscopy, and the average thickness of cell-cell junction within endothelial monolayer was measured from the obtained fluorescence images using ImageJ software.

2.4.2. huvEC monolayer maturity

Antithrombotic ability and cell quiescence state were analyzed to detect the maturity of the generated huvEC monolayer on the fibrous samples. huvECs were seeded onto the samples at a high density of 3×10^5 cells/cm^2 in 24-well plates to form a compact cell monolayer. To evaluate the antithrombotic ability of the regenerated cell monolayer, after culture for 3 days, 5 U/mL thrombin (Solarbio, China) was added to incubate the cellularized constructs for 15 min. Then, actin cytoskeleton and VE-cadherin expression of huvEC monolayer were stained following the protocols in Section 2.3.2 and **2.4.1**. Finally, the constructs were observed under laser-scanning confocal microscopy, and the averaged thickness of cell-cell junction was analyzed using ImageJ software. Regarding quiescent state examination of huvECs within cell monolayer, after culture for 1, 3, and 5 days, 300 μL of fresh hECM containing 5% CCK-8 (Beyotime, China) was used to incubate the cellularized constructs for 4 h at 37 °C. Thereafter, 100 μL of the solution were transferred into 96-well plate for absorbance measurements at 450 nm using a microplate reader.

To further verify the huvEC monolayer maturity, gene expression of endothelial function markers including *endothelial NO synthase (eNOS)*, *VE-cadherin*, *CD31*, and *biglycan* were analyzed by a quantitative real-time polymerase chain reaction (RT-qPCR) assay. Briefly, huvECs were seeded onto the fibrous scaffolds at a high density of 3×10^5 cells/cm^2 in 24-well plates to form a confluent cell monolayer. After culture for 3 days, total RNA was extracted from the cell monolayer using the Biozol reagent (Zrbiorise, Shanghai, China) according to the manufacturer's instruction. Thereafter, mRNA was reverse-transcribed into cDNA followed by standard qPCR analysis using qPCR kit (EZ Bioscience, China) according to the manufacturer's instruction using an ABI Sequence Detection System (Q6, Applied Biosystems, USA). All PCR results were normalized to the expression level of housekeeping gene GAPDH prior to further analysis. The primer sequences (Sangon Biotech, China) used for the real-time reverse transcription-PCR are listed in Table S1.

2.5. Capacity verification of the developed CAG@PLys@PDA-Cu^{2+} coating for in situ catalyzing NO generation for endothelial monolayer maturation

2.5.1. NO generation

Monitoring NO generation catalyzed by the fibrous scaffolds was carried out using a Griess Assay Kit (Beyotime, China) according to the manufacturer's instruction. In brief, the circular fibrous membranes were placed into 24-well plates, and then incubated for 100 min at 37 °C with 500 μL test PBS solution containing 10 μM NO donor S-Nitrosoglutathione (GSNO, Macklin, China) and 10 μM reducing agent glutathione (GSH, Macklin, China). During the incubation process, the real-time NO generation was monitored using Griess Assay Kit at 5-min intervals.

2.5.2. Promoting effect of the generated NO on endothelial monolayer integrity

huvECs at a high density of 3×10^5 cells/cm^2 were seeded onto the fibrous samples and cultured with flesh hECM containing 10 μM GSNO and 10 μM GSH for 3 days. Then, the effect of material-catalyzed NO release on huvEC monolayer integrity was examined by staining the actin cytoskeleton and VE-cadherin expression following the protocol in Section 2.3.2 and **2.4.1**. Lastly, the constructs were observed under laser-scanning confocal microscopy, and the averaged thickness of cell-cell junction was measured using ImageJ software.

2.5.3. Promoting effect of the generated NO on endothelial monolayer functions

CD31 expression and cell endocytosis ability were detected to evaluate the promoting effect of the generated NO on endothelial monolayer functions. To examine CD31 expression, huvECs were seeded onto the fibrous samples at a high density of 3×10^5 cells/cm^2, and then were cultured in fresh hECM or fresh hECM containing 10 μM GSNO and 10 μM GSH for 3 days. Thereafter, CD31 of the cell monolayer was stained with rabbit anti-CD31 antibody (1:200 dilution, Bioss, China) as the primary antibody and FITC-conjugated affinipure goat anti-rabbit IgG (H+L) as the secondary antibody. The detailed process was conducted following the protocol in Section 2.3.3. Afterwards, the constructs were observed under laser-scanning confocal microscopy, and the fluorescence intensity per cell was measured from the immunofluorescence images using ImageJ software ($n > 10$); To observe the cell endocytosis ability, huvECs were seeded on the samples at a low density of 3×10^4 cells/cm^2, and then were cultured in fresh hECM or fresh hECM containing 10 μM GSNO and 10 μM GSH for 3 days. After that, the cellularized constructs were incubated with 450 μL fresh hECM containing 30 μg/mL DiI-labeled human acetylated low-density lipoprotein (Ac-LDL, Yeason, China) for 4 h at 37 °C. Finally, the Ac-LDL uptake into huvEC cytoplasm was observed using laser-scanning confocal microscopy at an excitation wavelength of 550 nm, and the fluorescence intensity, normalized to single cells, was calculated using ImageJ software ($n = 8$).

2.6. Capacity verification of the developed CAG@PLys@PDA-Cu^{2+} coating for anti-thrombogenesis

2.6.1. Hemocompatibility

To evaluate the anticoagulant activity of pristine PLCL nanofibers, PDA-Cu^{2+} modified, PLys@PDA-Cu^{2+} modified, and CAG@PLys@PDA-Cu^{2+} modified nanofibers, fresh rabbit whole blood, in which clotting reaction has been activated by $CaCl_2$ aqueous solution (0.1 M), was used to immerse the fibrous samples (1 × 1 cm) for 10, 20, 30, 40, 50, and 60 min at 37 °C. At each time point, the samples ($n = 3$) were retrieved and incubated with 2.5 mL distilled water for 5 min, which allowed the hemolysis of the non-trapped red blood cells to release hemoglobin into the water. Then, the hemoglobin concentration was determined by measuring the absorbance at 545 nm with a microplate reader.

To analyze the hemocompatibility of the fibrous samples, measurement of activated partial thromboplastin time (APTT) and thrombin time (TT) was performed. Briefly, platelet poor plasma (PPP) was obtained by centrifuging fresh rabbit whole blood at 3000 rpm for 15 min. Then, 500 μL PPP was added to the samples that have been placed in 24-well culture plate for 30 min incubation at 37 °C. Afterwards, to examine APTT, 100 μL of the incubated PPP and 100 μL APTT reagent (Sunbio, China) were transferred to the test tube for 3 min incubation at 37 °C, followed by the addition of 100 μL $CaCl_2$ solution (0.025 M). The clotting time was then measured using an automatic blood coagulation analyzer (Rayto, USA). To examine TT, 100 μL of the incubated PPP and 100 μL TT reagent (Sunbio, China) were added to the test tube for 3 min incubation at 37 °C, followed by the measurement with the automatic blood coagulation analyzer.

2.6.2. Fibrinogen adsorption and conformational change

Immunochemistry was used to semi-quantitatively determine the amounts of the adsorbed fibrinogen (FGN) and denatured FGN (i.e., fibrinogen γ) on the fibrous samples. Briefly, 200 μL rabbit PPP was added to the circular samples in 24-well culture plate for 15 min incubation at 37 °C. To examine FGN adsorption, after being rinsed with PBS for 3 times, the samples were incubated with 200 μL mouse monoclonal anti-rabbit FGN antibody (1:100 dilution, Bioss, China) for 1 h at 37 °C, followed by the incubation of 200 μL horseradish peroxidase (HRP)-conjugated goat anti-mouse IgG antibody (1:200 dilution, Bioss, China) for 30 min at 37 °C. After that, 100 μL of 3,3′,5,5′-tetramethylbenzidine

(TMB) agent was added for 10 min, and then 50 μL H_2SO_4 solution (1 M) was used to stop the color reaction. Finally, 100 μL of the reaction solution was transferred to 96-well plate for absorbance measurements at 340 nm using a microplate reader. Similarly, examination of FGN conformational change was performed using mouse monoclonal anti-rabbit fibrinogen γ antibody (1:100 dilution, Bioss, China) following the aforementioned protocol.

2.6.3. Platelet adhesion and activation

Platelet adhesion and activation on the fibrous samples were observed using rabbit platelet-rich plasma (PRP) which was prepared by centrifuging rabbit whole blood at 250 g for 15 min [22]. Briefly, 200 μL PRP was added to the circular samples in 24-well culture plates for 1 h incubation at 37 °C. To examine the amount of adhered platelet on samples, 200 μL Triton X-100 (1%) was added to hemolyze platelets for 5 min, and then 20 μL lysate was transferred into a 96-well plate for further preparation. Finally, the platelet amount was quantified using lactate dehydrogenase (LDH) assay kit (Nanjing Jiancheng Bioengineering Institute, China) following the manufacturer's instructions, and the absorbance measurement was performed at 440 nm using a microplate reader; To detect platelet activation, the PRP-treated samples were fixed with 4% paraformaldehyde for 30 min, followed by the incubation of 10% goat serum for 1 h to block nonspecific adsorption. Thereafter, the samples were incubated with mouse anti-rabbit p-selectin monoclonal antibody (Cloud-clone Corp., China) for 1 h followed by FITC-conjugated goat anti-mouse IgG (Yeasen, China) for 30 min. Lastly, the samples were observed under laser-scanning confocal microscopy.

2.7. In vivo animal test

2.7.1. In vivo implantation

To verify the phase-adjusted endothelial healing *in vivo*, CAG@-PLys@PDA-Cu^{2+} modified micropatterned nanofibers (~90 μm membrane thickness) were constructed into small-diameter tubular grafts (2 mm inner diameter, 1 cm length, and 5 rolled layers) by rolling them up in the direction perpendicular to the microgroove axis, followed by seam-sealing with medical adhesive (name as M-PLCL). Meanwhile, pristine micropatterned PLCL nanofibers were chosen to fabricate small-diameter tubular grafts with similar size and used as control groups (name as PLCL). After that, the constructed grafts were implanted *in vivo* to repair a segmental defect of rabbit carotid arteries. Briefly, twenty-four healthy male New Zealand white rabbits (1.2–1.8 kg, all male, Shanghai Jiagan Biotechnology, China) were randomly divided into two groups (i.e., PLCL and M-PLCL), and then anesthetized by intramuscular injection of 0.8–1 mL anesthetic (Virbac Zoletil®50, France). After being completely unconscious, the heavy hair around rabbit neck was removed with depilatory cream, and the region of neck was disinfected followed by a skin incision to expose the left internal carotid artery. After transection of the exposed artery between two clamps, sterilized tubular grafts were implanted to bridge the defect by microsurgical suturing two ends with 9–0 monofilament nylon sutures. Then, the clamps were removed to restore the blood flow, and the wound was closed with 5–0 monofilament nylon sutures. Afterwards, the rabbits were individually caged for 1, 6, and 12 weeks to observe endothelial regeneration, vascular remodeling and anti-thrombogenesis in the implanted grafts. The animals were allowed for free movement and access of food and water. No anticoagulation and antiplatelet drugs were administrated during the whole process. In this study, animal experiment protocol was approved by the Animal Care and Experiment Committee of Shanghai Ninth People's Hospital, Shanghai Jiao Tong University School of Medicine.

2.7.2. Doppler ultrasound and SEM analyses

Patency of the implanted tubular grafts was analyzed by 3D ultrasonography and examination of real-time blood flow velocity using high-resolution ultrasound (Visualsonics, Canada) under anesthesia. To obtain SEM images of the graft inner surface, the rabbits were euthanized by intramuscular injection of overdosed chloral hydrate. Then, the implanted grafts were retrieved and dehydrated in a series of graded ethanol. After being dried at the critical point, the samples were sputter-coated with gold and observed by SEM.

2.7.3. Histological evaluation

To perform the histological analysis, the explanted grafts were harvested, fixed, dehydrated and embedded in paraffin for tissue section at 5 μm thickness. The tissue cross-sections were then stained with hematoxylin and eosin (H&E, Solarbio, China), Verhoeff-Van Gieson (Solarbio, China) for elastin, Masson's trichrome (Solarbio, China) for collagen, and Safranin O (Solarbio, China) for glycosaminoglycans (GAGs) according to product instructions. Lastly, histological images were digitally recorded under an inverted microscope (Nikon DS-Ri2, Japan), and luminal area was measured from the cross-sections stained with H&E.

2.7.4. Immunofluorescent staining

To perform immunofluorescent staining, the cross-sections of the explanted grafts were permeated by 0.2% Triton X-100 for 5 min and then blocked by 10% goat serum for 30 min at room temperature. After that, the cross-sections were incubated with the primary antibodies overnight at 4 °C, followed by the incubation of the secondary antibody for 2 h and DAPI for 10 min at room temperature. Concretely, to observe endothelial regeneration, ECs were stained with rabbit anti-CD31 antibody (1:200 dilution, Bioss, China); To detect the regeneration and maturity of smooth muscle cell (SMC) layer, SMCs were stained with rabbit anti-alpha smooth muscle actin (anti-α-SMA) antibody (1:200 dilution, Proteintech, USA) and mouse anti-smooth muscle myosin heavy chain (anti-SM-MHC) antibody (1:100 dilution, Arigo, China); To observe the graft-mediated inflammatory response, pro-inflammatory macrophages were stained with rabbit anti-inducible nitric oxide synthase (anti-iNOS) antibody (1:200 dilution, Bioss, China). After that, Alexa Fluor 594 goat anti-rabbit IgG (1:200, Invitrogen, USA) and Alexa Fluor 488 goat anti-mouse IgG (1:200, Invitrogen, USA) were used as the secondary antibodies, respectively. Lastly, the stained sections were observed under laser-scanning confocal microscopy. For quantitative analysis, the coverage rate of regenerated endothelium was calculated from the cross-sections stained with anti-CD31 antibody by summing the length of CD31-positive monolayer and dividing it by the total length of the cross-sections [22]; Regenerated SMC layer thickness was quantified from the cross-sections stained with anti-α-SMA antibody by ImageJ software; The positive areal ratio of SM-MHC/α-SMA was quantitatively measured from the cross-sections stained with anti-α-SMA and anti-SM-MHC.

2.8. Statistical analysis

All quantification data are presented as means ± standard deviation. The significant difference among multiple groups was detected with one-way ANOVA and then with Tukey's post hoc test for pair-wise comparisons using the Origin 9.0 software. A value of $^{*}p < 0.05$ or $^{**}p < 0.01$ was considered statistically significant.

3. Results

3.1. Surface chemistry of the CAG@PLys@PDA-Cu^{2+} modified PLCL nanofibers

Firstly, to verify the role of the CAG@PLys@PDA-Cu^{2+} coating in phase-adjusted endothelial healing, random PLCL nanofibers were used for the step-wise modification by PDA-Cu^{2+}, PLys, and CAG. Although pH 5.5 may slightly impair the PDA-Cu^{2+} coating during CAG grafting (Fig. S1A), SEM images confirmed the successful grafting of PDA-Cu^{2+} complexes, PLys molecules, and CAG peptides on the PLCL nanofiber

surface (Fig. 2A), with the average fiber diameter increased from 0.62 ± 0.10 μm (PLCL) to 0.86 ± 0.11 μm (PLCL@PDA-Cu@PLys@CAG) (Fig. S1B). The noted C, Cu, N, and S elements on the substrate surface of PLCL@PDA-Cu@PLys@CAG further evidenced the successful modification.

XPS and FTIR were performed to observe the changes in the chemical structure and composition of the substrates (Fig. S1C-**D**). The presence of new peaks of Cu2p element and S2p element revealed the successful modification of PDA-Cu^{2+} coatings and CAG molecules (Fig. 2B). Regarding the C/N atomic ratio of dopamine molecules (8:1) and PLys molecules (3:1), a significant decrease of C/N atomic ratio was noted in the spectrum of PLCL@PDA-Cu@PLys compared to that of PLCL@PDA-Cu. Additionally, the nitrogen atomic percentage also increased from 2.64 to 6.43% (Fig. S1E). These findings indicated the successful grafting of PLys molecules. Moreover, C1s core-level spectrum could be curve-fitted with four peaks at 288.8 eV (C═O), 286.5 eV (C–O), 285.5 eV (C–N), and 284.2 eV (C–C), and the N1s core-level spectrum could be curve-fitted with three peaks at 401.0 eV (−NH_2), 399.1 eV (−NH−), and 397.5 eV (−N =) (Fig. 2C) [44,45]. The –N = percentage significantly increased from 4.07% (PLCL@PDA-Cu) to 13.65% (PLCL@PDA-Cu@PLys) along with –NH− content decreasing from 84.81% to 67.76%, affirming that PLys was likely to be grafted to PDA-Cu^{2+} coating *via* more Schiff base reaction (generating –N = groups) than Michael addition reaction (forming –NH− groups)

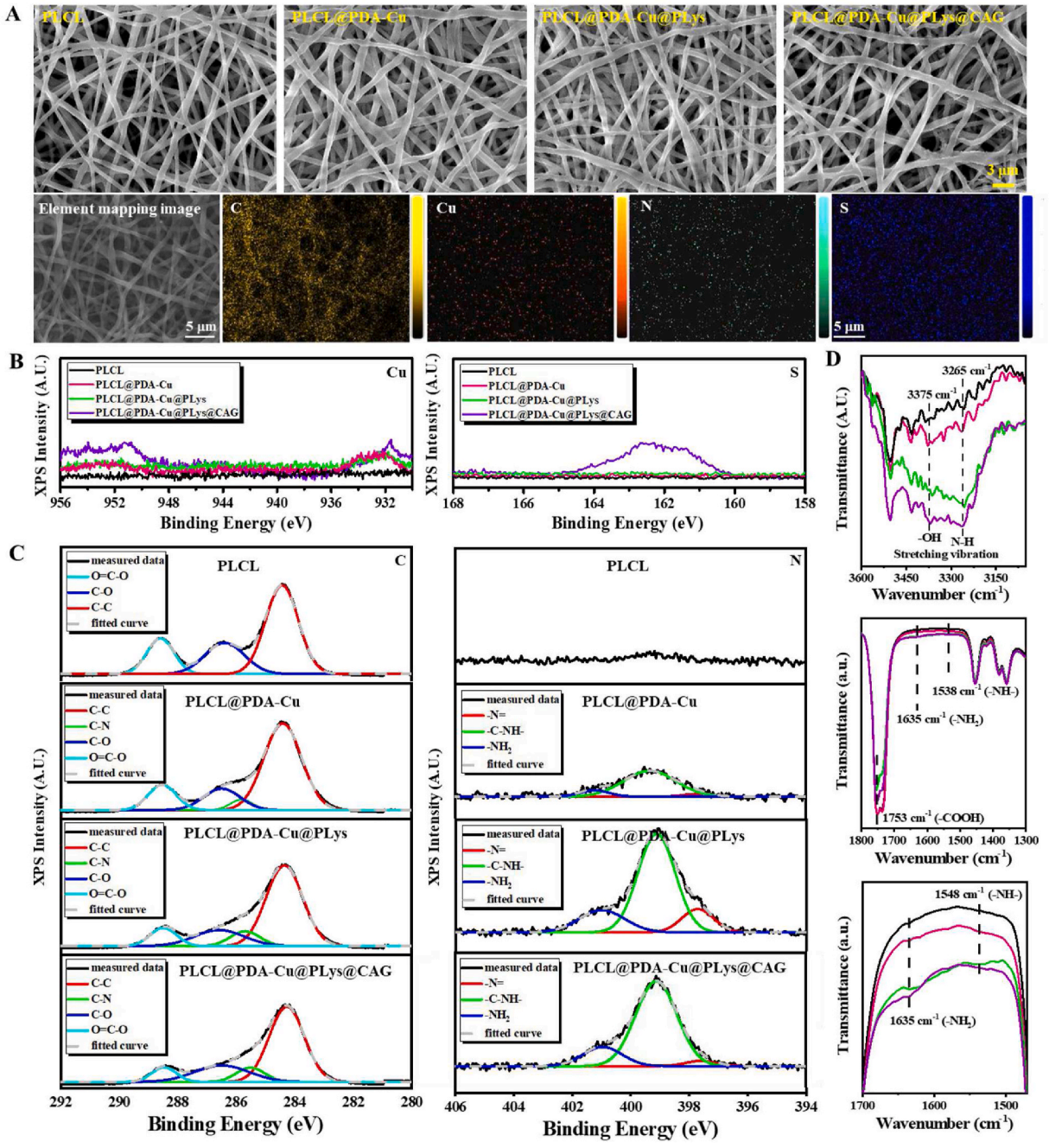

Fig. 2. Morphology and chemistry of random PLCL nanofibers after step-wise modifications of PDA-Cu^{2+} complexes, PLys molecules, and CAG peptides: (A) SEM images, and element mapping (C, Cu, N, and S) of CAG@PLys@PDA-Cu^{2+} modified nanofibers; (B) XPS spectra for Cu2p element and S2p element; (C) XPS spectra for the deconvolution of C1s and N1s peaks; (D) black, red, green and purple lines of FTIR spectra indicate PLCL, PLCL@PDA-Cu, PLCL@PDA-Cu@PLys, and PLCL@PDA-Cu@PLys@CAG, respectively.

Table 1
Surface functional group composition of different nanofibers.

Samples	Functional group composition(%)						
	C–C	C–N	C=O	C–O	-N =	-NH-	$-NH_2$
PLCL	57.02	–	24.11	18.86	–	–	–
PLCL@PDA-Cu	65.43	4.70	15.69	14.18	4.07	84.81	11.12
PLCL@PDA-Cu@PLys	63.20	9.49	16.98	10.33	13.65	67.76	18.59
PLCL@PDA-Cu@PLys@CAG	61.31	9.49	20.84	8.35	3.67	79.26	17.07

(Table 1). Compared to PLCL@PDA-Cu@PLys, after CAG grafting, both C═O and –NH– contents were increased while the C–O amount was decreased in the spectrum of PLCL@PDA-Cu@PLys@CAG, verifying the formation of amido bonds. Furthermore, from the FTIR spectra, the increased characteristic absorption peaks of –OH, N–H, –COOH, and $–NH_2$ reconfirmed the successful modification of CAG@PLys@PDA-Cu^{2+} on PLCL nanofibers (Fig. 2D).

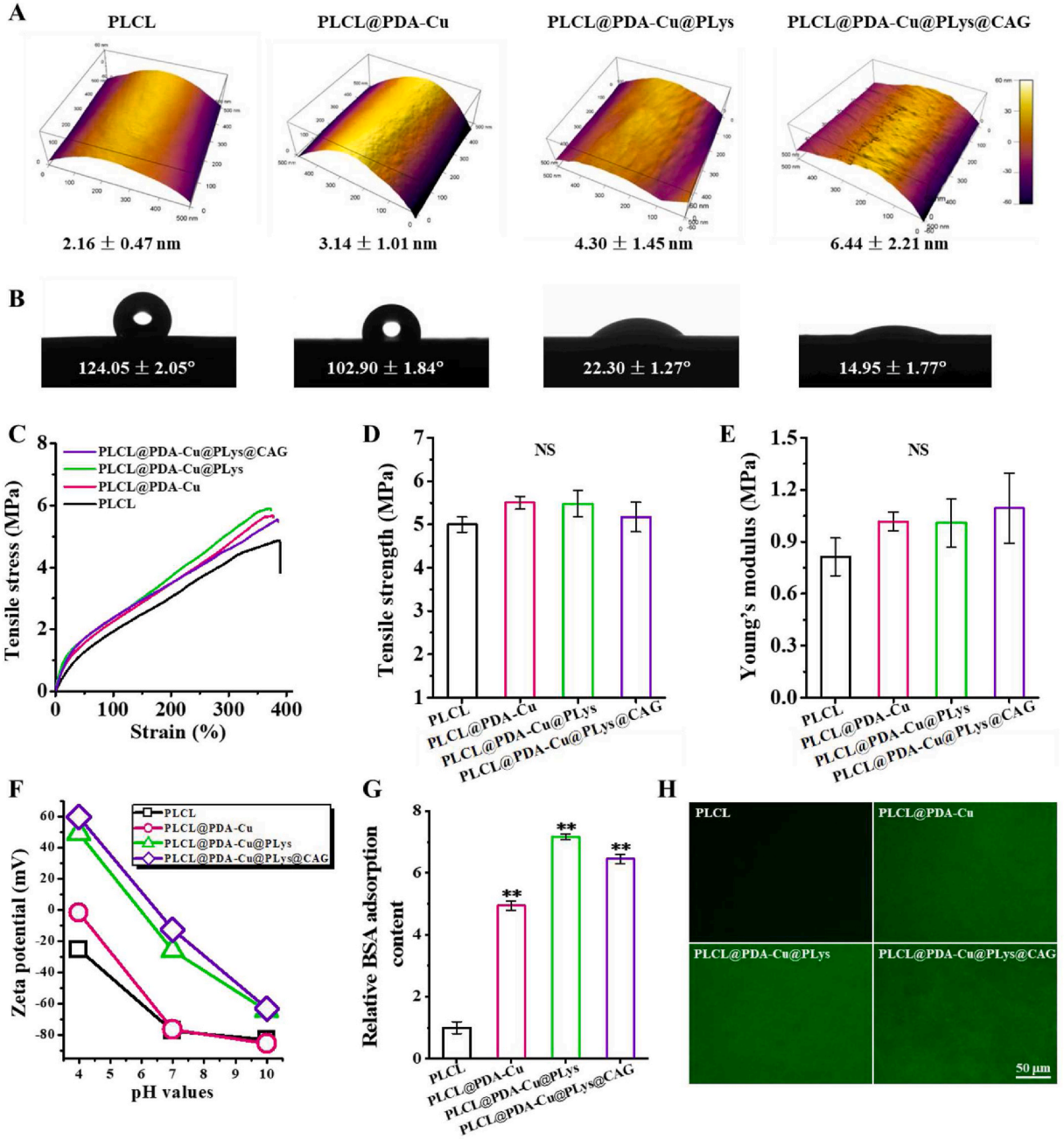

Fig. 3. Characterization of the random PLCL nanofibers after step-wise modifications of PDA-Cu^{2+} complexes, PLys molecules, and CAG peptides: (A) AFM images; (B) Surface wettability (n = 3); (C–E) Wet tensile property, including stress-strain curves, tensile strength, and Young's modulus (n = 6); (F) Zeta potential; (G–H) Relative BSA adsorption (n = 6) and FITC-BSA adsorption. $^{**}p < 0.01$.

3.2. Physicochemical properties of the CAG@PLys@PDA-Cu^{2+} modified PLCL nanofibers

Surface topography of single nanofiber was significantly affected by the step-wise modifications of PDA-Cu^{2+}, PLys, and CAG. As shown in Fig. 3A, pristine PLCL nanofibers presented a smooth surface with low fiber surface roughness of 2.16 nm. After PDA-Cu^{2+} coating, a distinct rugged surface (fiber surface roughness: 3.14 nm) was observed because of the accumulation of PDA nanoaggregates *via* non-covalent cross-linking (e.g., π-π stacking and hydrogen bonds) [22,46]. Such fiber surface heterogeneity was further increased with the fiber surface roughness increased to 4.30 nm (PLCL@PDA-Cu@PLys) as well as an ulterior increase in roughness to 6.44 nm (PLCL@PDA-Cu@PLys@CAG), likely attributing to the abundant grafting of linear molecules of PLys and CAG. Additionally, CAG@PLys@PDA-Cu^{2+} also appeared to affect the surface wettability of the nanofibers due to the introduction of plentiful hydrophilic groups, as the WCA value sharply reduced from 124.05° (PLCL) to 14.95° (PLCL@PDA-Cu@PLys@CAG) (Fig. 3B). For wet tensile property, all samples exhibited ~400% of strain at break (Fig. 3C), indicating their superior resilience. No significances in tensile strength and Young's modulus were observed, indicating that either PDA-Cu coating, PLys grafting, or CAG grafting had not influence on the wet tensile property of the PLCL nanofibers (Fig. 3D-E). For zeta potential analysis, the noted negative surface charge of pristine PLCL nanofibers could effectively facilitate the deposition of PDA-Cu^{2+} complexes that contain rich positive –NH_2 groups (Fig. 3F). Upon PLys and CAG grafting, the introduction of abundant positive-charged groups of –NH_2 and negative-charged groups of –COOH gave rise to the higher

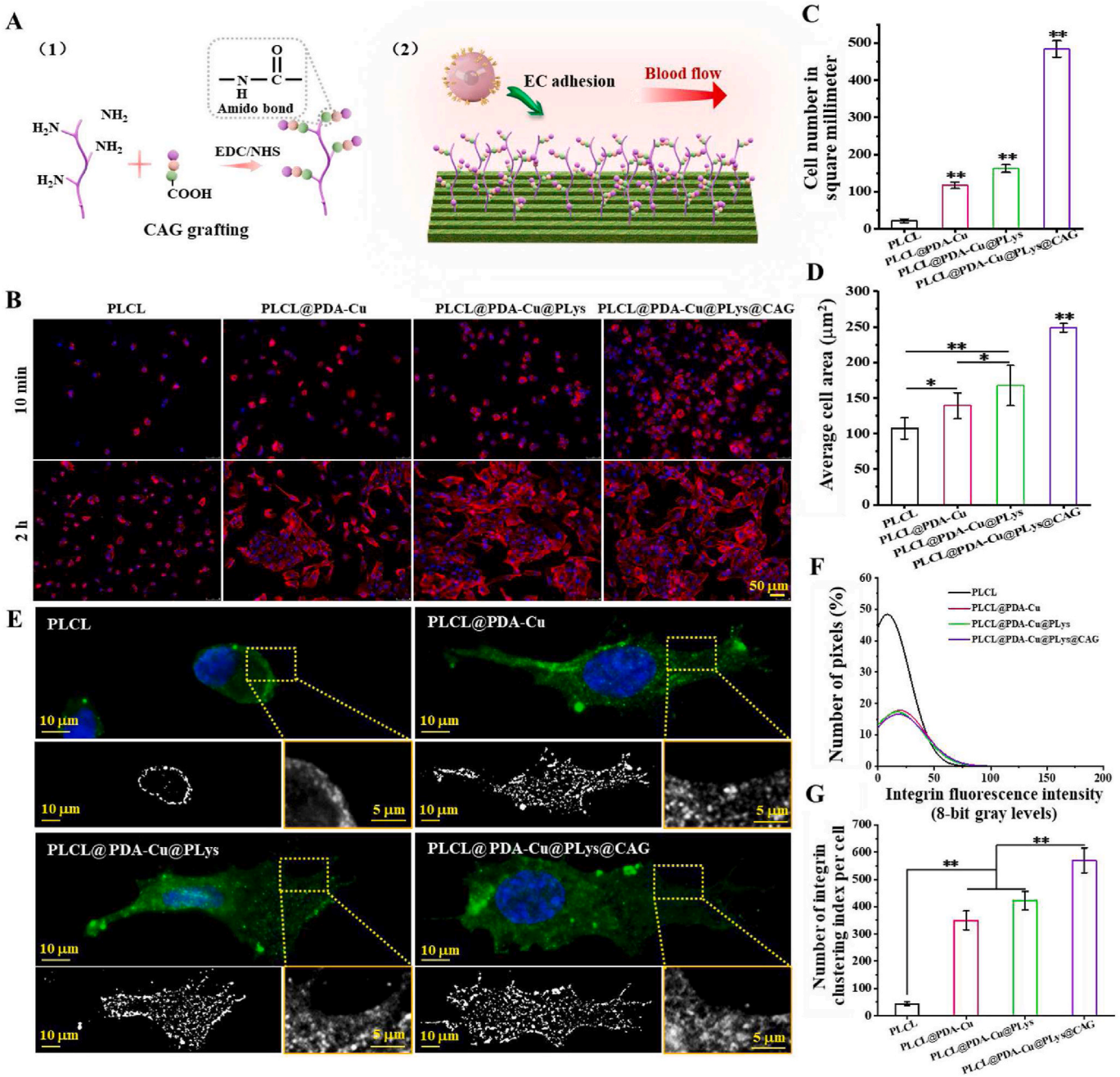

Fig. 4. Capacity of the CAG@PLys@PDA-Cu^{2+} modified PLCL nanofibers for EC capture: (A) Schematic diagrams of CAG grafting and EC capture; (B) Cell adhesion for 10 min and cell spreading for 2 h; (C–D) Quantified cell number and cell spreading area from image B (n = 10); (E) Immunofluorescence images of integrin β1; (F–G) Quantitative analysis of the FA size distribution and FA number per cell (n = 6). *$p < 0.05$; **$p < 0.01$.

zeta potential of the nanofibers. Besides, PDA-Cu^{2+} coating also significantly enhanced the protein adsorption capacity of the nanofibers when compared to pristine PLCL nanofibers (Fig. 3G). Interestingly, grafting of PLys was able to further improve the protein adsorption capacity, but the promoting effect was reduced by CAG grafting, indicating the higher protein adsorption capacity of PLys than CAG. Such a tendency was directly verified and reconfirmed by visual observation of the FITC-labeled BSA adsorption (Fig. 3H).

3.3. CAG@PLys@PDA-Cu^{2+} modification effectively promoted EC adhesion and spreading

As the EC-affinity peptides that were screened from collagen type IV [15], CAGs were grafted to PLys molecules *via* amido bonds for EC favoring niche modification (Fig. 4A). To verify the ability of CAG-modified nanofibers to capture ECs, the stimulating effect of CAG@PLys@PDA-Cu^{2+} modification on cell adhesion and spreading was observed (Fig. 4B). Compared to the pristine PLCL control, an inclination of ascending cell adhesion was found on the substrates after step-wise modification of PDA-Cu^{2+} complexes, PLys molecules and CAG peptides. Quantification of cell adhesion number indicated the

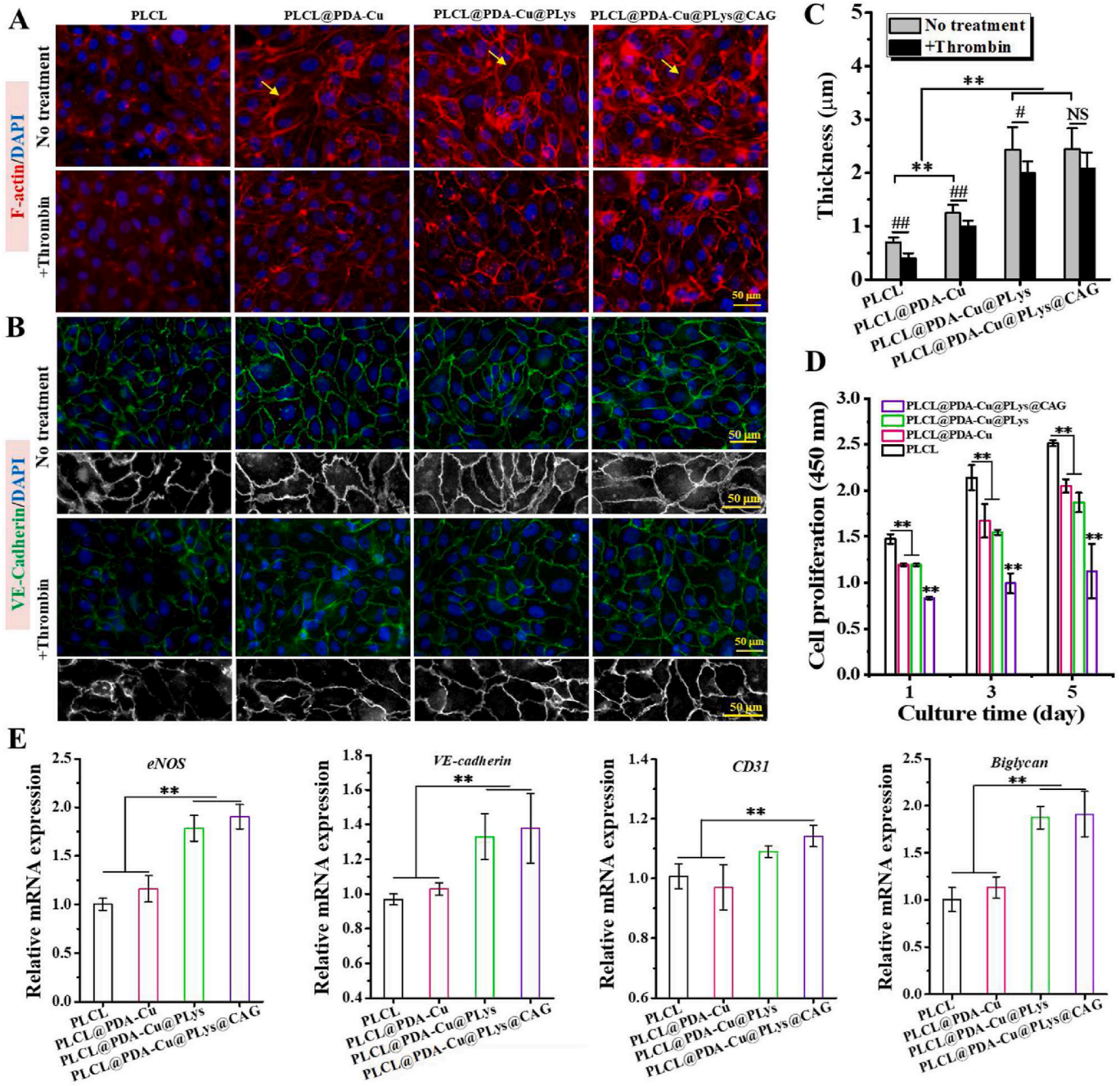

Fig. 5. Capacity of the CAG@PLys@PDA-Cu^{2+} modified PLCL nanofibers for inducing compact endothelial monolayer formation after 3 days of culture: (A) Cell morphology before and after thrombin treatment, yellow single-headed arrows indicate the cortical arcs of actin; (B) Fluorescence images of VE-cadherin (green) and DAPI stained nuclear (blue) before and after thrombin treatment; (C) Quantified thickness of cell-cell junctions from image B (n = 10); (D) Cell proliferation (n = 6); (E) Gene expression of huvEC function related markers (n = 3). $^{**}p < 0.01$; $^{\#} < 0.05$; $^{\#\#} < 0.01$; NS > 0.05.

tendency of huvECs to adhere in a quickest way on CAG-grafted nanofibers (Fig. 4C). After 2 h culture, both PDA-Cu^{2+} complexes and PLys molecules showed a predisposition of promoting more huvEC spreading in comparison to that of the pristine PLCL, which was further enhanced by CAG grafting (Fig. 4D). Overall, CAG@PLys@PDA-Cu^{2+} modification effectively promoted EC adhesion and spreading.

Focal adhesions (FAs), as the large protein complexes that tether cell cytoskeleton (e.g., integrins) to substrates (e.g., ligands) [18], play a critical role in guiding cell-matrix interaction. Given the excellent improvement for cell adhesion, CAG@PLys@PDA-Cu^{2+} coating was speculated to enhance cell-matrix interaction *via* triggering the FA site dynamics of huvECs. To verify this, integrin β1 expression of huvECs was determined (Fig. 4E). The results revealed that large-sized punctate FAs were mainly located at the peripheral region of cell body when huvECs were cultured on the pristine PLCL. After modification of PDA-Cu^{2+}, PLys, and CAG, more newly formed large-sized punctate FAs appeared around the central region of the cell bodies. In term of quantified distributions of punctate FAs, less small-sized punctate FAs were identified on PDA-Cu^{2+}, PLys, and CAG modified nanofibrous substrates than the FAs on pristine PLCL (Fig. 4F), but step-wise modifications of PDA-Cu^{2+} complexes, PLys molecules, and CAG peptides were inclined to increase FA number (Fig. 4G). All these evidences indicate that CAG@PLys@PDA-Cu^{2+} coating significantly improved FA site dynamics of huvECs.

3.4. CAG@PLys@PDA-Cu^{2+} modification markedly promoted the compact endothelial monolayer formation

The effect of CAG@PLys@PDA-Cu^{2+} modification on endothelial monolayer morphology was analyzed through fluorescence microscopy of phalloidin colocalized F-actin stress fibers. As shown in Fig. 5A, surface chemistry had an impact on cytoskeleton organization within the huvEC monolayer. Unlike the indistinguishable morphology of huvECs on pristine PLCL, confluent huvEC monolayer with strong peripheral cortical arcs around cell-cell contacts (yellow arrow) was formed on the PDA-Cu^{2+} modified substrates, suggesting the excellent cell-cell interaction in the huvEC monolayer [47]. A further scrutinization delineated an intensified organization of cortical arcs within huvEC monolayer after the grafting of PLys and CAG, demonstrating that CAG@PLys@PDA-Cu^{2+} modification markedly promoted the formation of a confluent and compact endothelial monolayer.

Expression of the junction protein VE-cadherin was further examined to confirm the integrity of the regenerated cell monolayer. As shown in Fig. 5B, huvEC monolayers on all fibrous scaffolds were visually integrated well with the neighboring cells, but a further close look into the cell-cell junctions (desaturated images) revealed that after step-wise modification of PDA-Cu^{2+} and PLys, cell-cell junctions in honeycomb-like structure became thicker and formed more stable reticular morphology, while no further improvement was observed after CAG grafting (Fig. 5C), indicating that the promoting effect of CAG@PLys@PDA-Cu^{2+} coating on cell-cell interaction for huvEC monolayer integrity was mainly attributed to PDA-Cu^{2+} complexes and PLys molecules.

The antithrombotic ability of the regenerated cell monolayer was also examined by observing the thrombin-mediated integrity of huvEC monolayer. It was found that F-actin amount in the huvECs was markedly reduced on all samples after thrombin treatment, but the regenerated huvEC monolayer on PLCL@PDA-Cu@PLys and PLCL@PDA-Cu@PLys@CAG still showed strong cortical arcs around cell-cell junctions, exhibiting an excellent antithrombotic ability (Fig. 5A). To quantify the cell-cell junction variation, VE-cadherin expression was further examined by immunofluorescent staining. The results showed that after thrombin treatment, cell-cell junctions became thinner on all samples (Fig. 5B-C). However, given the loss of cell-cell junction between the adjacent cells on PLCL and PLCL@PDA-Cu groups, the retained reticular morphology of endothelial monolayer on PLCL@PDA-Cu@PLys@CAG indicated that CAG@PLys@PDA-Cu^{2+} coating markedly enhanced the antithrombotic ability of huvEC monolayer.

High integrity of endothelial monolayer is always accompanied with significant endothelium quiescence of ECs to inhibit unwarranted cell expansion [48]. To confirm it, huvEC proliferation of endothelial monolayer was examined by CCK-8. As shown in Fig. 5D, the cell density was demonstrated to increase by 45.15% on PLCL, 39.96% on PLCL@PDA-Cu, 38.98% on PLCL@PDA-Cu@PLys, and 19.29% on PLCL@PDA-Cu@PLys@CAG after 3 days of culture, and respectively increased by 70.52%, 71.74%, 68.21%, and 35.25% after 5 days of culture. These results implicated that after the endothelial monolayer formation, CAG@PLys@PDA-Cu^{2+} coating could effectively modulate the phenotype of confluent huvECs towards a quiescence state, although it was noted to exhibit a promoting effect on huvEC proliferation before endothelial monolayer formation (Fig. S2). Moreover, the gene expression related to endothelial functions (*eNOS*, *VE-cadherin*, *CD31*) and ECM secretion (*biglycan*) were also examined to verify the effect of CAG@PLys@PDA-Cu^{2+} modification on endothelial functions. Compared to the pristine PLCL control, several folds of increases in the concerned gene expression analysis were noted on the CAG@PLys@PDA-Cu^{2+} modified samples (Fig. 5E), including *eNOS* (1.90 ± 0.12 *vs* 1.00 ± 0.06), *VE-cadherin* (1.37 ± 0.20 *vs* 0.99 ± 0.03), *CD31* (1.14 ± 0.04 *vs* 1.00 ± 0.04), and *biglycan* (1.91 ± 0.24 *vs* 1.01 ± 0.12). All the data testified the capacity of CAG@PLys@PDA-Cu^{2+} modification for promoting the formation of compact endothelial monolayer as well as endothelial functions.

3.5. CAG@PLys@PDA-Cu^{2+} modification effectively catalyzed NO generation to accelerate endothelial maturity

Give the capacity of Cu^{2+} to generate NO *via* decomposing GSNOs (an endogenous RSNO species) according to the reaction 2GSNO → 2NO + GSSG (Fig. 6A) [49], we speculated that CAG@PLys@PDA-Cu^{2+} modification could effectively catalyze NO generation. To verify this, samples were immersed in PBS with donor supplements for 100 min (Fig. 6B). Compared to pristine PLCL, the interposition of PDA-Cu^{2+} significantly increased NO release and the NO releasing amount rose linearly within 20 min, demonstrating the robust NO catalytic activity. However, after continuous immersion in PBS solution for 100 min, the NO releasing amount was noted to increase slightly, indicating the decrease of NO production rate that was attributed to the consumption of the NO donor in the reaction chamber. Moreover, after PLys grafting, no significant change in the NO catalytic capacity disclosed the retained NO catalytic activity, but the subsequent CAG grafting apparently reduced the catalytic capacity, perhaps because of the blocking of partial catalytic sites by CAG peptides. Nevertheless, CAG@PLys@PDA-Cu^{2+} coating still exhibited an excellent NO catalytic activity.

To examine the effect of the generated NO on endothelial monolayer integrity and maturity, huvECs were cultured in hECM with the presence of NO-donor supplements. As shown in Fig. 6C, cell morphology of the huvEC monolayer formed on pristine PLCL surface showed no obvious differences from that of the huvECs cultured in hECM without NO-donating supplements (see Fig. 5A) after 3 days of culture. Differently, more clarity of honeycomb-like structure was observed in the regenerated huvEC monolayer on the PDA-Cu^{2+} modified nanofibers after the addition of NO-donor supplements. Meanwhile, more newly and thicker stress fibers also appeared in the central region of huvEC body on the PLys@PDA-Cu^{2+} modified and CAG@PLys@PDA-Cu^{2+} modified nanofibers. These findings indicated that the NO generation strongly improved endothelial integrity. Endothelial monolayer maturity was further examined by analyzing the state of cell-cell junctions (Fig. 6C). After the addition of NO-donor supplements, huvEC monolayer was visually integrated well with the neighboring cells on all samples, but thicker cell-cell junctions were identified in the huvEC monolayer on all Cu^{2+} contained nanofibers (Fig. 6C–D *vs* Fig. 5A). In contrast, no significant difference was observed on pristine PLCL groups (Fig. 6D),

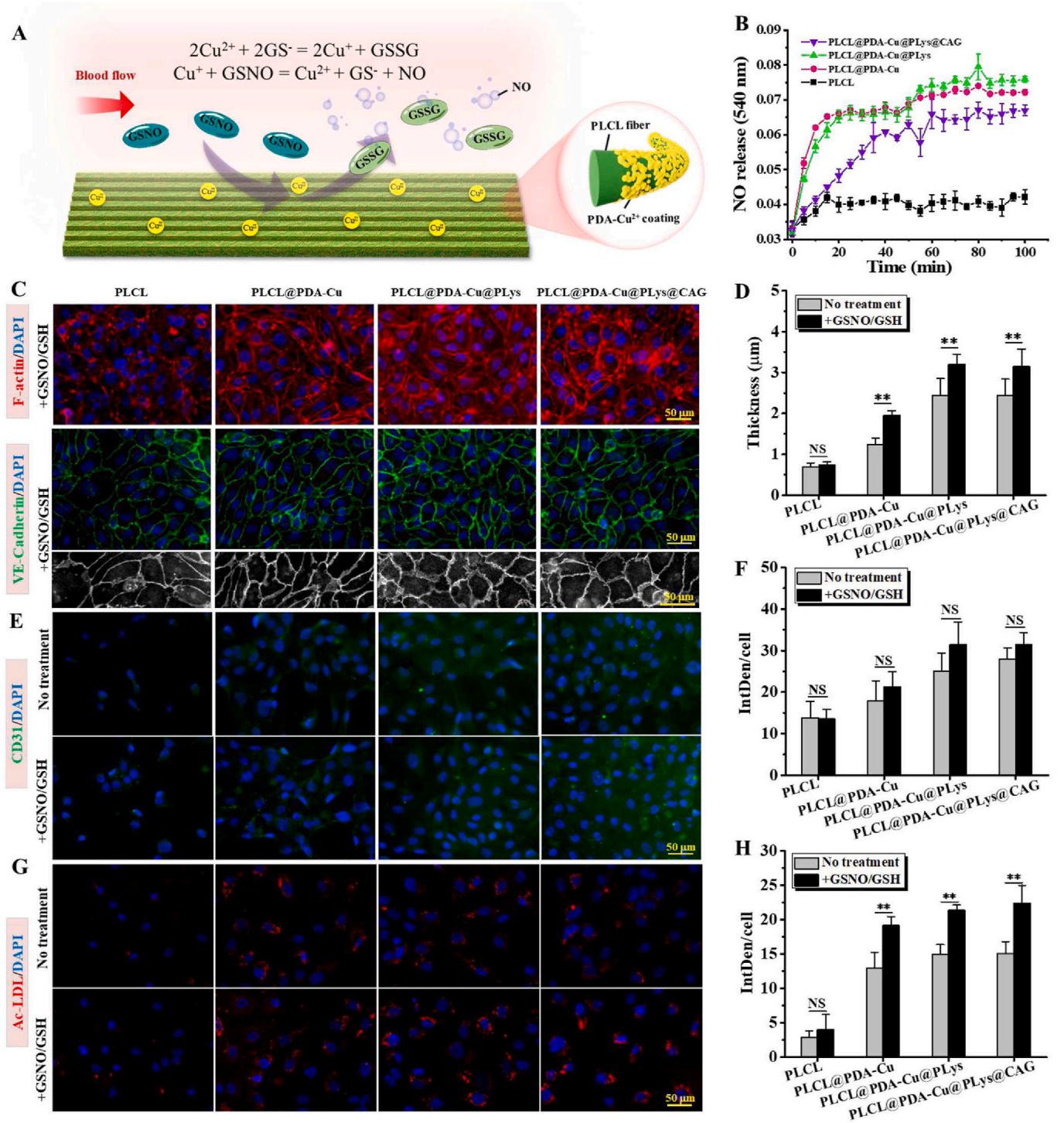

Fig. 6. Capability of CAG@PLys@PDA-Cu^{2+} modified PLCL nanofibers to *in situ* catalyze NO generation for endothelial maturation: (A) Schematic diagram of NO generation; (B) Monitoring NO generation by Griess assay (n = 3); (C) Cell morphology and VE-cadherin expression of huvECs with the presence of NO-donor supplements for 3 days. F-actin (red), VE-cadherin (green), and nuclear (blue); (D) Quantified thickness of cell-cell junctions from image C (n = 10); (E&F) Immunofluorescence and quantified fluorescence intensity of CD31 with and without NO-donor supplements for 3 days (n = 6); (G&H) Immunofluorescence and quantified fluorescence intensity of Ac-LDL uptake with and without NO-donor supplements for 3 days (n = 6). $^{**}p < 0.01$; NS > 0.05.

indicating that CAG@PLys@PDA-Cu^{2+} modification could effectively catalyze NO generation to promote cell-cell interaction for endothelial monolayer integrity and maturity.

Additionally, CD31 (an antithrombotic molecule) and Ac-LDL uptake (a critical indicator related to cell endocytosis ability) were further examined to investigate the impact of the generated NO on endothelial function. CD31 expression was found to be numerically higher on all Cu^{2+} contained nanofibers after the addition of NO-donor supplements than that without NO-donor supplements, although the difference was not statistically significant (Fig. 6E-F, $p > 0.05$). Nevertheless, after the addition of NO donors, distinct increases of Ac-LDL uptake were identified in the huvEC monolayer on all Cu^{2+} contained nanofibers rather than pristine PLCL (Fig. 6G-H), reaffirming the ability of CAG@PLys@PDA-Cu^{2+} modification to offer an effective NO catalytic activity

for *in situ* NO generation, thus accelerating the endothelial maturation.

3.6. CAG@PLys@PDA-Cu^{2+} modification significantly enhanced substrate antithrombogenicity

PLys can be grafted to PDA-incorporated coating *via* Schiff base and Michael addition reactions, and the resultant functionalized coating was speculated to enhance substrate antithrombogenicity through selectively binding plasminogen (Fig. 7A). Given that thrombogenesis is usually associated with blood component destruction, plasma protein adsorption, and platelet adhesion/activation [50], a series of hemocompatibility related biological assays were performed to obtain insight into the effect of CAG@PLys@PDA-Cu^{2+} modification on substrate anti-thrombogenic properties, including erythrocytes-concerned hemocompatibility, FGN adsorption and conformation change, as well as blood platelet adhesion and activation. For kinetic clotting time, higher absorbance resulting from more free hemoglobin in the solution indicates less clotting [22]. The apparent improvement of absorbance revealed that PLys grafting tended to induce less clot formation than pristine PLCL and PDA-Cu^{2+} modified nanofibers, although CAG grafting slightly weakened its inhibitory effect on clot formation (Fig. 7B). Such tendency was further verified by APTT and TT results (Fig. 7C-D), in which APTT and TT correspond to the activity of blood to coagulate *via* coagulation pathways and the capacity of thrombin-mediated fibrin polymerization [51]. These findings indicated that PLys grafting could significantly enhance the antithrombogenicity of the substrates, which grant CAG@PLys@PDA-Cu^{2+} modification with excellent anti-coagulation capability.

Material-stimulated thrombogenesis includes the activation of a series of inter-connected processes, such as protein adsorption, platelet adhesion and activation, platelet aggregation, and FGN polymerization [50]. As one of the representative plasma proteins that mediate platelet adhesion and thrombus [52], FGN adsorption and conformation change were examined to understand the antithrombogenicity of

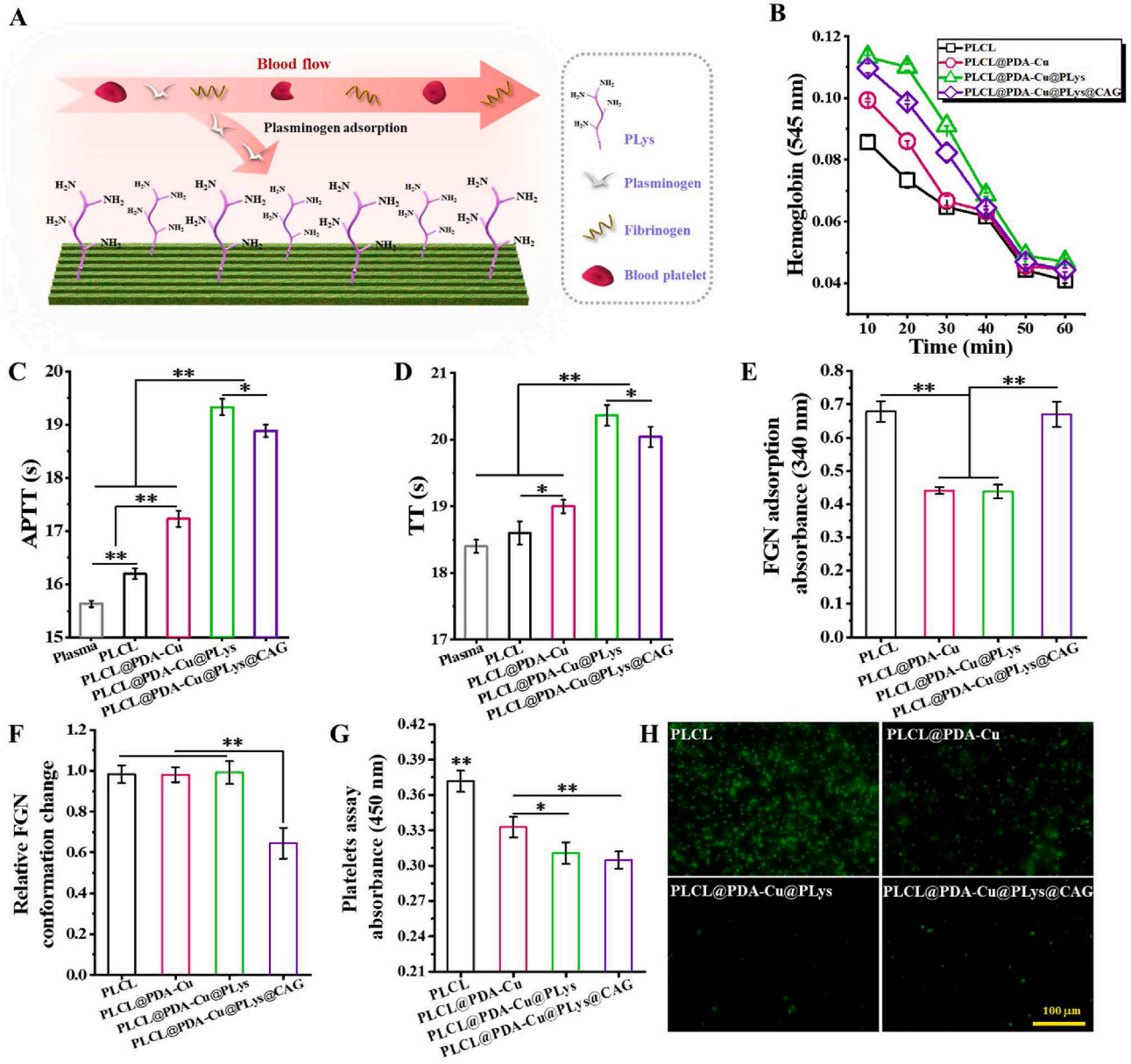

Fig. 7. Capacity of the CAG@PLys@PDA-Cu^{2+} modified PLCL nanofibers for inhibiting thrombogenesis: (A) Schematic diagram; (B) The kinetic clotting time for 60 min (n = 3); (C–D) Clotting times for APTT and TT (n = 3); (E–F) FGN adsorption and the relative conformation change normalized to PLCL control (n = 3); (G–H) Platelet adhesion by LDH assay and activation by p-selectin immunofluorescence staining (n = 3). *$p < 0.05$; **$p < 0.01$.

CAG@PLys@PDA-Cu^{2+} modification. Compared to PLCL control, both PDA-Cu^{2+} complexes and PLys molecules effectively inhibited FGN adsorption without influence on relative FGN conformation change (Fig. 7E-F). Although higher capacity for FGN adsorption was observed after CAG grafting, the CAG@PLys@PDA-Cu^{2+} coating supplied the excellent capacity for conformational preservation (i.e., less denaturation) in FGN. Previously, FGN adsorption and denaturation have been shown to promote platelet adhesion and activation *via* selectively blocking the GPIIb/IIIa receptors of platelets [53,54]. This explained the descending tendency of adhered platelet number on the substrates after step-wise modifications of PDA-Cu^{2+}, PLys, and CAG (Fig. 7G). Much less extent of platelet activation on these substrates were also demonstrated by the immunostaining of p-selectin images (Fig. 7H).

3.7. CAG@PLys@PDA-Cu^{2+} modified micropatterned nanofibers effectively achieved rapid endothelialization and inhibited acute thrombosis within 1 week in vivo

Precisely-designed micropatterned nanofibers were previously successfully fabricated by combining electrospinning and soft lithography (Fig. S3A) [55]. Similarly fabricated nanofibers in this study not only exhibited the surface high-resolution parallel microgrooves (Fig. S3B-C), but also significantly induced the formation of native-like endothelium with oriented morphology (Fig. S3D). The small-diameter tubular grafts rolled by the membrane and seam-sealed with medical adhesive exhibited excellent structural stability (Fig. S3E-F). Afterwards, the gross appearance of the small-diameter vascular grafts and rabbit carotid artery replacement surgery was carried out as shown in Fig. 8A. All implanted vascular grafts remained patent without bleeding and rupture subsequent to the restoration of blood flow and pressure. At 1-week post-implantation, Doppler ultrasound observed the excellent patency

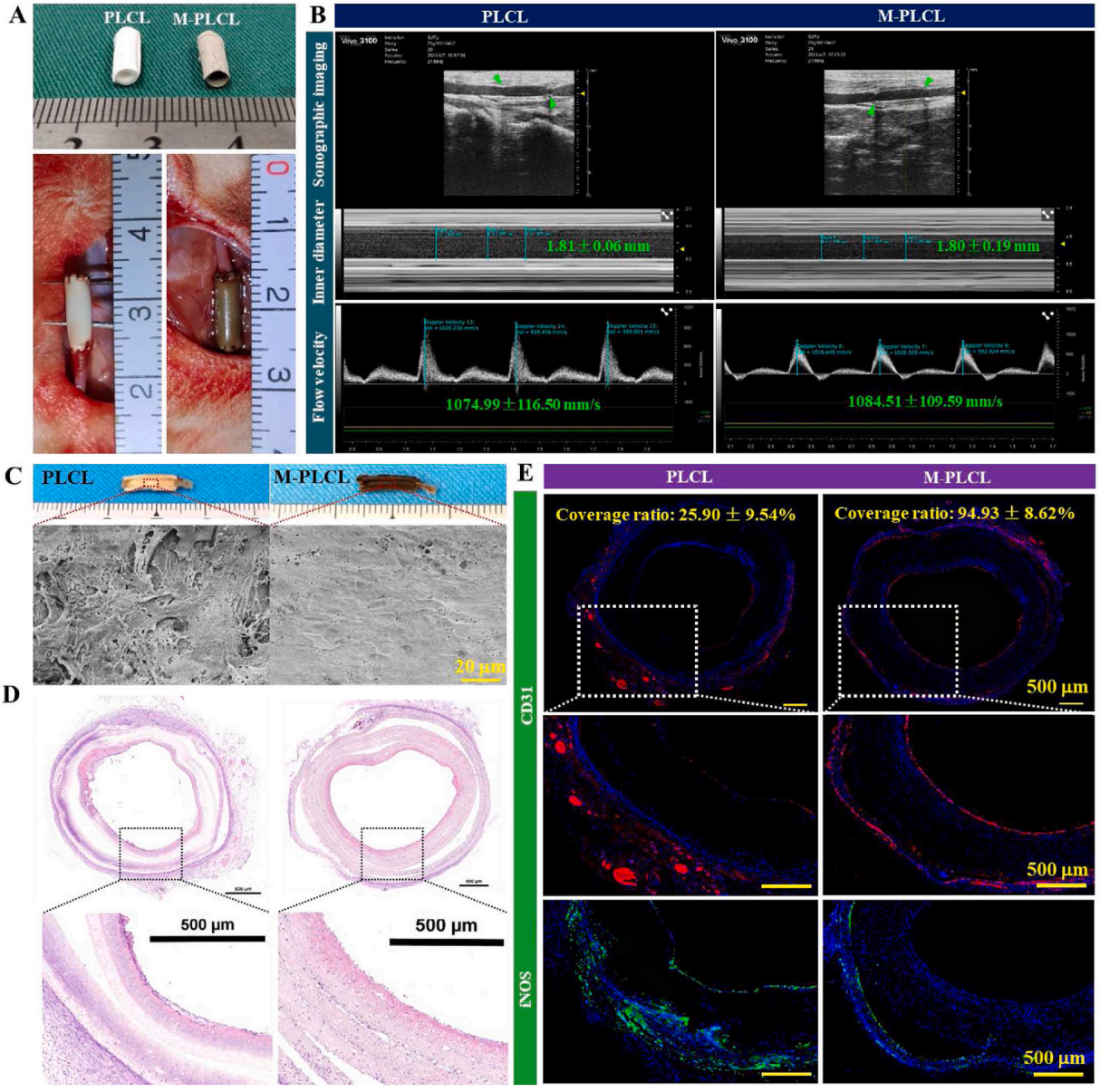

Fig. 8. Assessment of the effectiveness in achieving rapid endothelialization and inhibiting acute thrombosis on the CAG@PLys@PDA-Cu^{2+} modified PLCL nanofibers (middle part) at 1-week post-implantation: (A) Gross view of the engineered small-diameter vascular grafts and rabbit carotid artery replacement surgery; (B) Sonographic images of the implanted vascular grafts (n = 3), green arrows indicate the graft position; (C) Gross view and SEM images of the luminal surfaces; (D) H&E staining of the cross-sectioned grafts; (E) Immunofluorescence staining of CD31 and iNOS of the cross-sectioned grafts.

without aneurysm and occlusion in all implanted grafts, and PLCL and M-PLCL groups presented similar lumen diameter and flow velocity (Fig. 8B). Although the gross view of the graft internal surface found no obvious blood coagulation on both PLCL and M-PLCL, a close SEM examination revealed the evident unevenly distributed cells (SMC-like morphology) on the PLCL surface accompanied with the adhesion of abundant blood platelets (Fig. 8C). By contrast, the lumen surface of M-PLCL was largely covered by a confluent and oriented cell monolayer that were free of platelet aggregates (Fig.8C and Fig. S4).

H&E staining images further verified the presence of adhered blood platelets on PLCL lumens along with the presence of some subtle granula (Fig. 8D). To verify the rapid endothelializaiton on M-PLCL lumens, immunofluorescence staining of CD31 was performed. As shown, a confluent monolayer of cells with strong positive expression of CD31 was visible on M-PLCL (Fig. 8E), with 94.93 ± 8.62% endothelial coverage rate, indicating the high efficiency of M-PLCL in rapid endothelialization. Excessive inflammation also contributes to serious vascular complications [6]. Although extensive iNOS-positive macrophages appeared within graft walls of both PLCL and M-PLCL, PLCL grafts were noted to recruit more proinflammatory macrophages than M-PLCL grafts, indicating that CAG@PLys@PDA-Cu^{2+} modification could effectively resolve the inflammatory reaction. Besides, the homogeneous cell distribution within M-PLCL grafts also indicated the efficacy of CAG@PLys@PDA-Cu^{2+} modification in guiding cell growth into graft inside, as shown in H&E staining and immunofluorescence staining images.

3.8. CAG@PLys@PDA-Cu^{2+} modified micropatterned nanofibers effectively accelerated vascular regeneration after 6 weeks of in vivo implantation

To determine the vascular remodeling, the organization and composition of ECM were observed *via* histological staining after 6 weeks of implantation (Fig. 9A). Although gross view of all harvested

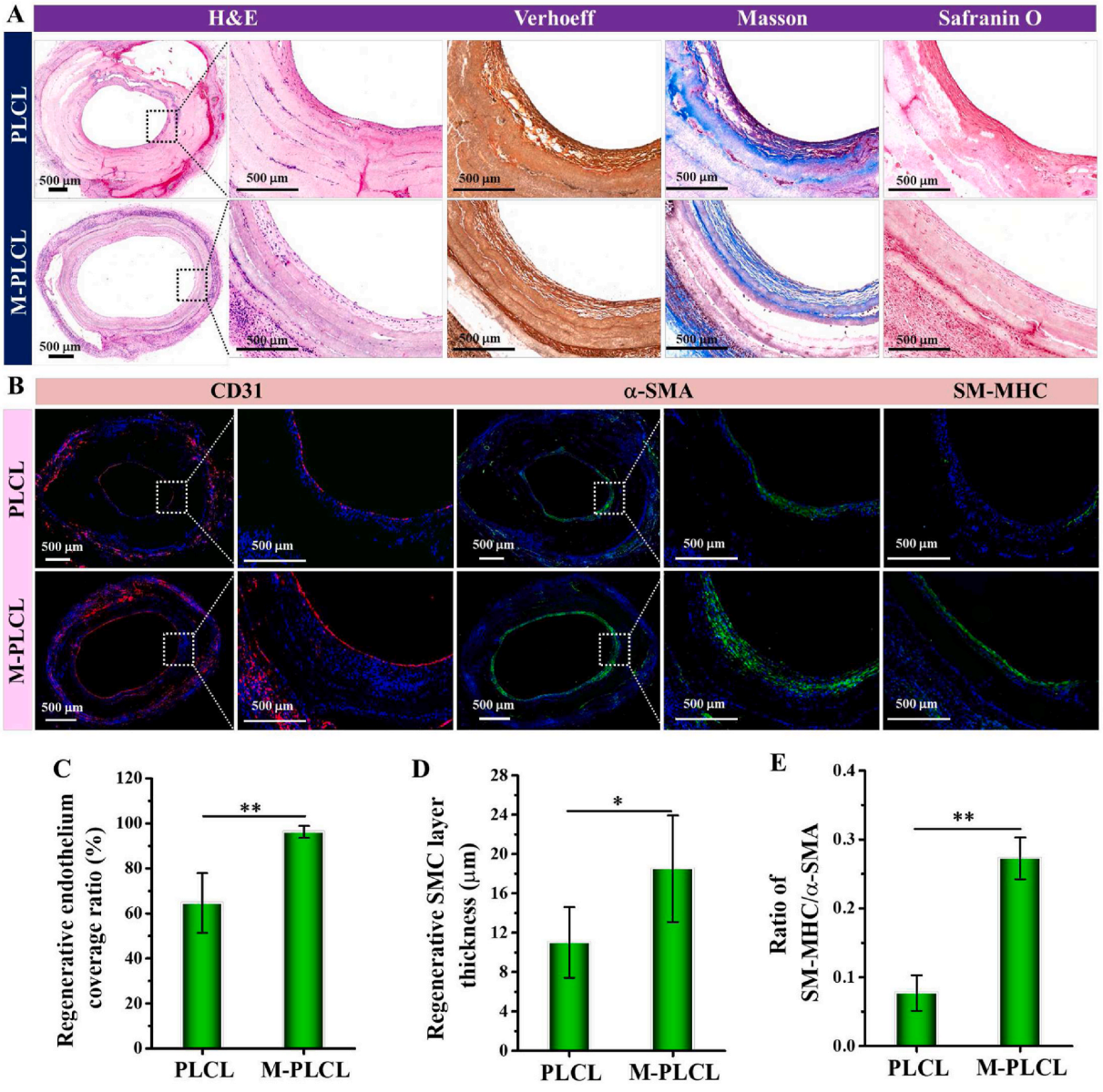

Fig. 9. Assessment of ECM deposition and vascular regeneration in the CAG@PLys@PDA-Cu^{2+} modified PLCL nanofibers (middle part) after *in vivo* implantation for 6 weeks: (A) H&E, Verhoeff-Van Gieson, Masson's trichrome, and Safranin O staining of the cross-sectioned grafts; (B) Immunofluorescence staining of CD31, α-SMA, and SM-MHC in the cross-sectioned grafts; (C–E) Quantitative analyses of the regenerated endothelium coverage ratio, SMC layer thickness, and ratio of SM-MHC/α-SMA (n = 3). *$p < 0.05$; **$p < 0.01$.

graft showed patent lumens, histological staining results demonstrated that compared to the disorganized ECM on PLCL inner surface, the regenerated tissue layer on the surface of M-PLCL graft lumen exhibited an artery-like ECM with an obvious circumferential orientation. As Verhoeff, Masson and Safranin O staining images displayed, well-organized elastin and collagen fibrillar ECMs were obviously formed in the regenerated tissue layer of M-PLCL grafts accompanied with the wide distribution of GAGs. Interestingly, a prolonged implantation for 6 weeks was demonstrated beneficial for the positive endothelial regeneration on PLCL, as evidenced by the increase of endothelium coverage

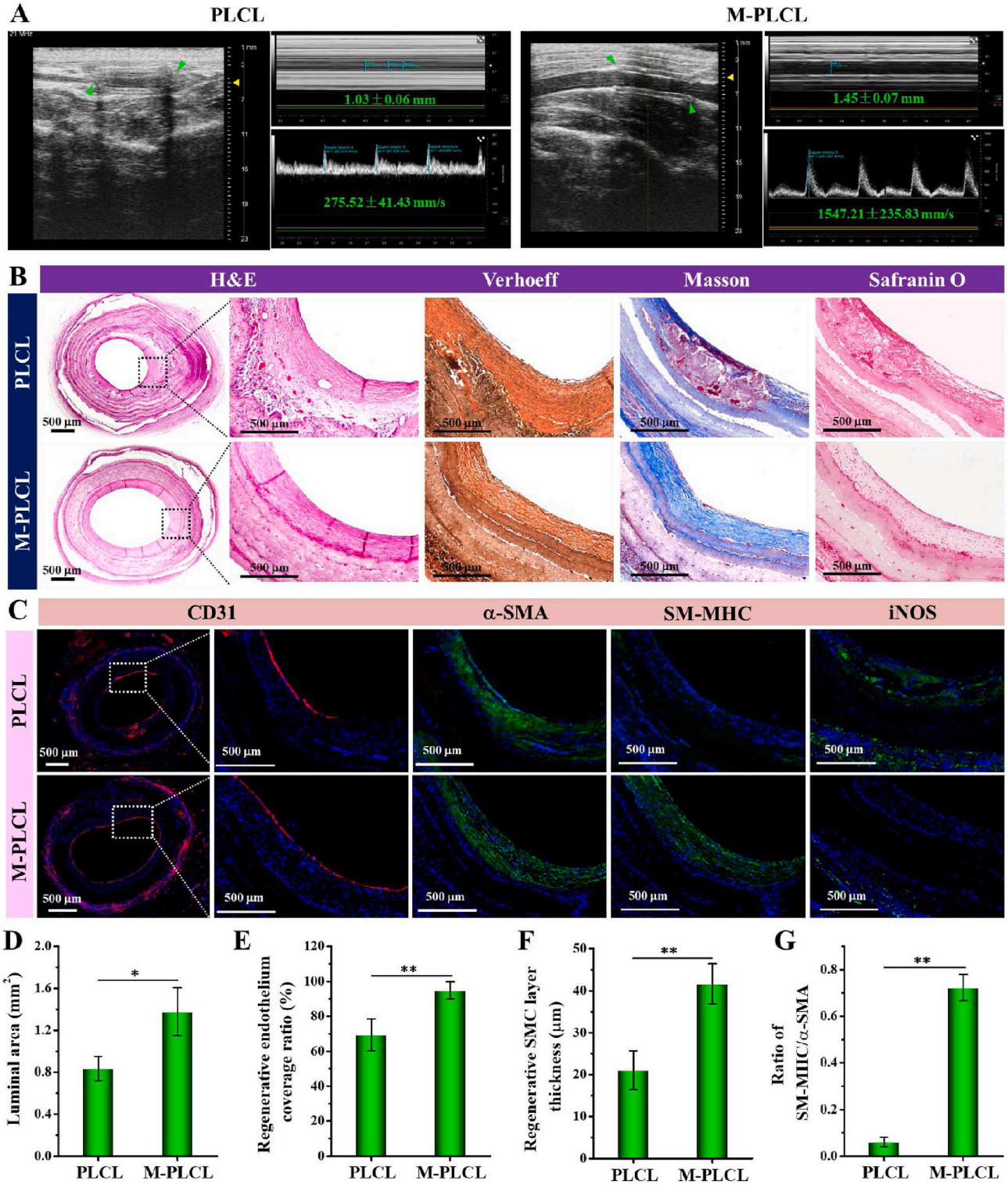

Fig. 10. Assessment of vascular maturation in the CAG@PLys@PDA-Cu^{2+} modified grafts (middle part) at 12-weeks post-implantation: (A) Sonographic images of the implanted vascular grafts (n = 3), green arrows indicate the graft position; (B) H&E, Verhoeff-Van Gieson, Masson's trichrome, and Safranin O stainings of the cross-sectioned grafts; (C) Immunofluorescent stainings of CD31, α-SMA, SM-MHC, and iNOS in the cross-sectioned grafts; (D) Quantification of cross-sectioned luminal area of the implanted grafts based on the H&E images (n = 3); (E–G) Quantification of the regenerated endothelium coverage ratio, SMC layer thickness, and ratio of SM-MHC/α-SMA of the cross-sectioned grafts (n = 3). *$p < 0.05$; **$p < 0.01$.

from 25.89 ± 9.54% (1 week, Fig.8E) to 64.62 ± 13.28% (6 weeks, Fig. 9C). Nevertheless, the endothelialization ratio was still far below the almost complete endothelial coverage of 96.20 ± 2.66% presented on M-PLCL (6 weeks, Fig. 9C). As for SMC layer remodeling, M-PLCL presented an outstanding inductive effect on guiding SMCs to regenerate a complete and thick α-SMA-positive SMC layer in the grafts after 6 weeks of implantation, whereas a discontinuous thin layer of α-SMA-positive SMCs was noted in PLCL grafts (Fig. 9B, D). To identify the maturity of the regenerated SMC layer, immunostaining of late contractile SMC marker SM-MHC was performed (Fig. 9B). In M-PLCL graft, the complete circle of mature SMCs occurred at the superficial surface of the regenerated SMC layer underneath the regenerated endothelium, suggesting the critical role of rapid endothelialization in promoting regeneration and maturation of a complete SMC layer (Fig. 9B). Furthermore, compared to the imperceptible SM-MHC expression in PLCL grafts, the appearance of more mature SMCs in M-PLCL indicated the high maturity of the regenerated SMC layer induced by CAG@-PLys@PDA-Cu^{2+} coating, which was further evidenced by a higher ratio of SM-MHC/α-SMA in M-PLCL group, an indicator of SMC layer maturity (Fig. 9E).

3.9. CAG@PLys@PDA-Cu^{2+} modified micropatterned nanofibers effectively improved vascular maturation after 12 weeks of in vivo implantation

After 12 weeks of implantation *in vivo*, Doppler ultrasound was performed to observe the patency of the implanted grafts. As shown in Fig. 10A, although both PLCL (3/4) and M-PLCL (4/4) maintained patent, the flow velocity in M-PLCL grafts was significantly higher than that of PLCL grafts (1547.21 ± 235.83 *vs* 275.52 ± 41.43 mm/s), likely caused by the bigger lumen diameter (Fig. 10A) and the larger luminal area (Fig. 10D). Through H&E staining examination, obvious blood clots appeared in the regenerated tissue on PLCL lumens (Fig.10B and Fig. S5A), representing a high risk in eliciting thrombogenesis-resultant vascular occlusion. In contrast, positive vascular remodeling was evidenced by the increase of regenerated tissue thickness in M-PLCL constructs, which shows compact multicellular layers in a circumferential orientation. In terms of the organization and composition of ECM in the regenerated vessels, Verhoeff, Masson and Safranin O stainings reconfirmed the well-aligned elastin and collagen fibers, and wide distribution of CAGs in the regenerated tissue layer of M-PLCL group, which differ from the noted formation of blood clots and disordered deposition of ECMs in PLCL grafts. Besides, the collagen I and laminin expressions in M-PLCL were also significantly higher than those in PLCL (Fig. S5B). Nevertheless, positive endothelial remodeling was still observed on PLCL lumens (Fig. 10C) with endothelial coverage rate increased from ~64.62% at 6 weeks (Fig. 9C) to 69.35 ± 9.17% at 12 weeks (Fig. 10E). Meanwhile, SMC layer regeneration (positive for α-SMA) was also observed (Fig. 10C) with SMC layer thickness significantly increased from 11.01 ± 3.58 μm (6 weeks) to 21.11 ± 4.58 μm in PLCL and from 18.50 ± 5.42 μm (6 weeks) to 41.67 ± 4.74 μm in M-PLCL (Fig. 9D vs Fig. 10F). Despite this, less maturation of SMC layer still appeared in PLCL grafts. Interestingly, the maturity of the regenerated SMC tissue in the M-PLCL was observed extending from the layer near to endothelium towards the inner part of the scaffold (Fig. 9B vs Fig. 10C). Together with the increase of SM-MHC/α-SMA ratio from 0.27 ± 0.03 (6 weeks, Fig.9E) to 0.72 ± 0.06 (12 weeks, Fig. 10G), these findings revealed that M-PLCL efficiently promoted the generation and maturation of SMC tissue. Furthermore, apparent expression of iNOS around the PLCL grafts indicated the persistence of pro-inflammation process *in vivo* even after 12 weeks of implantation. On the contrary, M-PLCL grafts exhibited an indiscoverable inflammatory response to vascular remodeling (Fig. 10C). Overall, all the findings indicated the occurrence of progressive and positive remodeling in the implanted M-PLCL grafts.

4. Discussion

Regeneration and maturation of native-like endothelium are crucial for material-guided vascular regeneration [3]. Although remarkable achievements have been made in the past, severe occlusion remains the top reason for the failures in material-guided vascular regeneration *in vivo* due to the incapability of the scaffold to achieve healthy endothelium remodeling [5,56], particularly in small-diameter vascular grafts (φ < 4 mm). This indicates that the currently developed strategies remain limited in inducing endothelial healing. In this study, inspired by the interconnected biological events of material-guided endothelial regeneration [7,8,57], we proposed a novel strategy of programming endothelial healing on graft surfaces by step-wise modifications of the micropatterned PLCL nanofibers with PDA-Cu^{2+} complexes, PLys molecules and CAG peptides. This proposed strategy was demonstrated to integrate multiple functions into a vascular graft, including high selective affinity for ECs, anisotropic contact guidance, GPx-like catalytic activity, and extraordinary antithrombogenicity. *In vivo*, these synergetic virtues were verified to successfully accelerate native-like endothelium regeneration within a short time, and effectively suppressed thrombogenesis for positive vascular remodeling.

CAG@PLys@PDA-Cu^{2+} modification can combine EC capture ability, NO interfacial catalytic release and antithrombogenic capacity to provide vascular grafts with multiple functions in a unique way. For example, given the strong adhesion and metal coordination abilities of PDA film [32], metal-phenolic network of PDA-Cu^{2+} complexes was successfully deposited on the PLCL nanofibers first *via* simple "one-pot" co-polymerization, as demonstrated by the appearance of Cu element in XPS spectrum (Fig. 2B) and increased surface roughness (Fig. 3A). During the PDA polymerization process, copper ions were mainly chelated with the phenolic hydroxyl groups of dopamine derivatives to form bis- and tris-catechol complexes [58]. Interestingly, this novel one-pot co-deposition strategy not only effectively develops a NO-catalytic surface (Fig. 6), but also allows the secondary grafting of amine-containing biomolecules *via* Schiff base and Michael addition reactions. Thus, the plasminogen-affinity PLys molecules were subsequently grafted to the substrates by using PDA-Cu^{2+} coating as the linker and coating matrix, and more Schiff base reaction than Michael addition reaction was confirmed to guide the PLys grafting (Fig. 2C and Table 1), which is consistent with Lys-mediated PDA polymerization [22]. Meanwhile, attributing to the long-chain structure and abundant hydrophilic groups of PLys molecules, both surface roughness and surface wettability of the substrate were enhanced after PLys grafting (Fig. 3A-B). Lastly, as the PLys@PDA-Cu^{2+} coating retained plentiful amino groups in the side chains of PLys which act as effective linkage points for the carboxyl-containing molecules, the high ECs-affinity peptide CAG was chosen to graft to the coating *via* EDC/NHS reaction due to their low adhesive tendency towards SMCs [16]. Collectively, based on the rational design, the functionalization of CAG@PLys@PDA-Cu^{2+} coating was successful added to the modified PLCL nanofibers which exhibited excellent elasticity and adjustable properties (e.g., strength and degradation rate) that are well-suitable for constructing small-caliber vascular grafts [6,59].

This special modification was confirmed capable of programmatically regulating endothelium regeneration through guiding cell adhesion, promoting confluent cell monolayer formation, inducing endothelium maturation as well as suppressing thrombosis (Figs. 4–7). *In vivo*, material-mediated endothelialization (i.e., endothelia healing) was recognized to involve a series of interconnected biological events [60]. Among them, cell homing/adhesion is the first key cellular event in endothelia healing. PDA-Cu^{2+} coating has the capability to effectively promote EC adhesion because of the phenolic/quinone groups of PDA and the presence of Cu^{2+} [58]. Certainly, as PDA has a specific reactivity for sulfhydryl- or amine-contained biomolecules, the increased adsorption of serum proteins to PDA-Cu^{2+} surface also serves as EC adhesion sites for cell adhesion [53]. After PLys grafting, the introduction of

abundant positively charged amine groups can further offer a better microenvironment to support EC adhesion and growth [53]. More interestingly, CAG is the basic component in type IV collagen and can selectively promote EC adhesion *via* transmembrane proteins such as integrins [16]. Hence, the highest level of EC adhesion was observed on the CAG@PLys@PDA-Cu^{2+} modified nanofibers (Fig. 4), thereby supporting an effective platform to cross the first hurdle of rapid endothelialization. Noteworthily, although excessive grafting of CAGs may affect the endothelial maturity likely due to the higher capacity of PLys than CAG for promoting EC functions (Fig. S6), appropriate CAG grafting was realized to improve EC capture and adhesion while retain cell functions (Fig. 5) *via* decreasing the EDC/NHS reaction time to 2 h. After cell adhesion, the micropatterned nanofibers could effectively induce the formation of endothelial monolayer with native-like morphology *via* contact guidance (Fig. S3). Based on the sufficient softness of nanofibers, this particular modification also provided the potential to enhance cell-matrix interaction for endothelial monolayer maturation [21]. In addition, the PDA-Cu^{2+} complexes with long-term catalytic activity of NO release are capable of accelerating rapid endothelialization as well, ascribing to the unique biological features of NO in promoting EC adhesion and function [61]. These evidences indicate that a confluent native-like endothelial monolayer formation can be effectively promoted on CAG@PLys@PDA-Cu^{2+} modified micropatterned nanofibers after EC recruitment and adhesion. Furthermore, once the compact endothelial monolayer was formed, the *in situ* generated NO could significantly promote endothelial maturation for healthy endothelial remodeling (Fig. 6). In general, vascular injury during graft implantation will inevitably activate strong coagulation reaction to motivate platelets adhesion and activation before endothelialization, which also constitutes a limitation on successful implantation of vascular grafts [50]. In this work, compared to pristine PLCL, CAG@PLys@PDA-Cu^{2+} coating was demonstrated to exhibit high protein adsorption capacity (Fig. 3G-H), because of its abundant active groups and non-covalent/covalent functionalities such as amine, hydroxyl groups and π-π bonds, which can interact with the amino acids involved in protein structure [62]. Theoretically, this surface may be coated with plasma proteins after being exposed to the human plasma. However, the plasma environment is complicated, and the presence of Cu^{2+} and PLys will first stimulate the specific adsorption of some proteins, such as certain selenoproteins (e.g., GPx), Cu^{+}/Cu^{2+}-containing enzymes, and plasminogen [22,63], which ultimately restrict the plasma protein adsorption and provide an antithrombotic surface [58,64], as shown in Fig. 7. Furthermore, NO generation can inhibit thrombogenesis *via* NO-cyclic guanosine monophosphate (cGMP) signaling pathway [26], and PLys grafting can further enhance the antithrombogenicity of substrates attributing to the excellent hemocompatibility, the presented steric exclusion and bound hydration, and the capacity for selectively binding plasminogen. All of them synergistically minimize erythrocyte destruction, restrain platelet adhesion and inhibit clot formation [22,49]. Overall, this strategy exhibits an excellent antithrombotic activity and phase-adjusted capacity for endothelium regeneration by combining the biological functions of anisotropic topography, PDA-Cu^{2+} complexes, PLys molecules and CAG peptides.

As expected, CAG@PLys@PDA-Cu^{2+} modified micropatterned nanofibers successfully fulfilled the rapid endothelialization within a short time after *in vivo* implantation, and exhibited a progressive and positive vascular remodeling during 12 weeks post-implantation (Figs. 8–10). This excellent vascular remodeling can be ascribed to the desired endothelium regeneration, inhibited adhesion of platelets and SMCs, and reduced inflammatory responses. As proven in this study, the resultant endothelialization rate (e.g., ~95% of endothelial coverage rate at 1 week, Fig. 8E) not only outperforms the counterpart group of PLCL (~26% at 1 week), but also surpasses the PDA-Lys coated materials (~87%, 4 weeks) [22], arginine-glycine-aspartic acid (RGD)-fused mussel adhesive proteins coated substrates (incomplete endothelial coverage, 4 weeks) [65], and PDA-bivalirudin-REDV modified grafts (~70%, 12 weeks) [66] reported in other studies. Since rapid formation of complete and well-functioning endothelium is critical for antithrombosis and pro-maturation of SMC tissue [67], the maturity of the regenerated SMC tissue on M-PLCL was found to start from the layer nearby regenerated endothelium (Fig. 9B). Meanwhile, attributing to the presence of PDA-Cu^{2+} complexes, PLys molecules and CAG peptides, M-PLCL exhibits an outstanding potential to inhibit SMC adhesion, prevent platelet aggregation and suppress blood clot formation. Thus, few platelets and SMCs were observed to adhere on M-PLCL (Fig. 8C). By contrast, the lumen surface of PLCL was covered by an incomplete endothelial cell monolayer with the adhesion of abundant blood platelets and SMC-like cells, which necessarily initiates a cascade of coagulation pathways to induce a severe thrombosis [67,68]. Hence, an apparent clot formation was observed in PLCL after 12 weeks of implantation (Fig. 10B). Additionally, the untrammeled acute inflammation phases caused by graft implantation (Fig. 8E) are usually short, lasting no longer than 2 weeks [69]. The persistent appearance of inflammation will suppress endothelial regeneration and accelerate clot formation [70]. This indicates that the occurrence of delayed inflammatory responses in PLCL during 12 weeks post-implantation (Fig. 10C), likely caused by the accumulation of acidic degradation products of PLCL [71], may also restrain vascular remodeling. However, in M-PLCL groups, the abundant amide groups of PLys can effectively neutralize the acidic environment to alleviate the inflammatory responses and inflammation-associated thrombosis. Besides, both NO generation and PDA coating can also alleviate the inflammatory response to some extent [22,26].

Summarily, the main objective of this study is to confirm the feasibility of CAG@PLys@PDA-Cu^{2+} modified micropatterned nanofibers to programmatically regulate EC behaviors for endothelial healing without inflicting thrombosis. Despite the generally achieved goal, this study still has several limitations. Firstly, the suggested strategy was performed based on a definite combination with certain component content. To achieve the desired effect of the organized modification on guiding vascular regeneration, further research should be carried out to ensure the optimum formula of PDA-Cu^{2+} complexes, PLys molecules, and CAG peptides. Secondly, while the grafting of CAG significantly accelerated EC adhesion, it also impaired the partial functionality of PLys molecules in mediating vascular remodeling to a certain extent. Therefore, more suitable molecules or peptides should be exploited in further researches for the graft modification. Despite the weakness, this study still supports an affirmation that step-wise modification of the micropatterned nanofibers with PDA-Cu^{2+} complexes, PLys molecules, and CAG peptides provides an effective strategy to achieve phase-adjusted endothelial healing without the risk of inflicting thrombosis in engineering a highly challenging small-caliber vascular graft.

5. Conclusion

Different from previous studies involving mono-phase manipulation of endothelium regeneration, this study successfully developed a novel strategy to achieve phase-adjusted endothelial healing. The yielded vascular grafts not only effectively promoted cell adhesion, accelerated confluent endothelial monolayer formation, and improved the regenerated monolayer maturation *in vitro*, but also effectively accelerated vascular regeneration with native-like tissue formation and long-term patency *in vivo*. Therefore, this study offers vital evidences to prove the effectiveness of programmed regulation of EC behaviors in endothelial healing. It also provides valuable insight into the design of biomimicking small-caliber vascular grafts towards the regeneration of functional blood vessels. Furthermore, attributing to the availability and simplicity of PDA coating onto various material surfaces, we envision that the PDA-based modification can be further extended to modify other blood-contacting synthetics.

Ethics approval and consent to participate

Animal experiment protocol was approved by the Animal Care and Experiment Committee of Shanghai Ninth People's Hospital, Shanghai Jiao Tong University School of Medicine (license number: HKDL [2018] 234).

CRediT authorship contribution statement

Bingcheng Yi: Conceptualization, Funding acquisition, Data curation, Formal analysis, Writing – original draft, Writing – review & editing. **Boya Zhou:** Animal tests, Investigation, Writing – original draft. **Zhenfeng Song:** Animal tests, Investigation. **Lei Yu:** Animal tests, Investigation. **Wenbo Wang:** Animal tests, Investigation, Validation, Writing – review & editing. **Wei Liu:** Resources, Supervision, Funding acquisition, Project administration, Writing – review & editing.

Declaration of competing interest

The authors declare that they have no known competing financial interests or personal relationships that could have appeared to influence the work reported in this paper.

Acknowledgements

This work was supported by National Key Research and Development Program of China (2018YFC1105800 to WL), China Postdoctoral Science Foundation (2020M681322 to BY), and National Natural Science Foundation of China (31870967 to WL and 81701841 to WW). We are also grateful to Shiyanjia Lab (www.shiyanjia.com) for its kind help in drawing schematic illustrations.

Appendix A. Supplementary data

Supplementary data to this article can be found online at https://doi.org/10.1016/j.bioactmat.2022.07.010.

References

[1] S.F. Rodrigues, D.N. Granger, Blood cells and endothelial barrier function, Tissue Barriers 3 (2015), 978720.
[2] A.N. Lyle, W.R. Taylor, The pathophysiological basis of vascular disease, Lab. Invest. 99 (2019) 284–289.
[3] R.J. Smith Jr., B. Nasiri, J. Kann, D. Yergeau, J.E. Bard, D.D. Swartz, S. T. Andreadis, Endothelialization of arterial vascular grafts by circulating monocytes, Nat. Commun. 11 (2020) 1622.
[4] H. Chang, M. Hu, H. Zhang, K. Ren, B. Li, H. Li, L. Wang, W. Lei, J. Ji, Improved endothelial function of endothelial cell monolayer on the soft polyelectrolyte multilayer film with matrix-bound vascular endothelial growth factor, ACS Appl. Mater. Interfaces 8 (2016) 14357–14366.
[5] Y. Zhuang, C. Zhang, M. Cheng, J. Huang, Q. Liu, G. Yuan, K. Lin, H. Yu, Challenges and strategies for in situ endothelialization and long-term lumen patency of vascular grafts, Bioact. Mater. 6 (2021) 1791–1809.
[6] M. Zhu, Y. Wu, W. Li, X. Dong, H. Chang, K. Wang, P. Wu, J. Zhang, G. Fan, L. Wang, J. Liu, H. Wang, D. Kong, Biodegradable and elastomeric vascular grafts enable vascular remodeling, Biomaterials 183 (2018) 306–318.
[7] J.V. Serbo, S. Gerecht, Vascular tissue engineering: biodegradable scaffold platforms to promote angiogenesis, Stem Cell Res. Ther. 4 (2013) 8.
[8] D. Pankajakshan, D.K. Agrawal, Scaffolds in tissue engineering of blood vessels, Can. J. Physiol. Pharmacol. 88 (2010) 855–873.
[9] A.J. Melchiorri, N. Hibino, J.P. Fisher, Strategies and techniques to enhance the in situ endothelialization of small-diameter biodegradable polymeric vascular grafts, Tissue Eng. B Rev. 19 (2013) 292–307.
[10] H. Savoji, M. Maire, P. Lequoy, B. Liberelle, G. De Crescenzo, A. Ajji, M. R. Wertheimer, S. Lerouge, Combining electrospun fiber mats and bioactive coatings for vascular graft prostheses, Biomacromolecules 18 (2017) 303–310.
[11] T. Zhu, H. Gu, H. Zhang, H. Wang, H. Xia, X. Mo, J. Wu, Covalent grafting of PEG and heparin improves biological performance of electrospun vascular grafts for carotid artery replacement, Acta Biomater. 119 (2021) 211–224.
[12] J.A. Hubbell, S.P. Massia, N.P. Desai, P.D. Drumheller, Endothelial cell-selective materials for tissue engineering in the vascular graft via a new receptor, Bio Technol. 9 (1991) 568–572.
[13] S.P. Massia, S.S. Rao, J.A. Hubbell, Covalently immobilized laminin peptide tyr-ile-gly-ser-arg (yigsr) supports cell spreading and colocalization of the 67-kilodalton laminin receptor with alpha-actinin and vinculin, J. Biol. Chem. 268 (1993) 8053–8059.
[14] K. Kanie, Y. Narita, Y. Zhao, F. Kuwabara, M. Satake, S. Honda, H. Kaneko, T. Yoshioka, M. Okochi, H. Honda, R. Kato, Collagen type IV-specific tripeptides for selective adhesion of endothelial and smooth muscle cells, Biotechnol. Bioeng. 109 (2012) 1808–1816.
[15] W. Du, C. Gao, Selective adhesion and directional migration of endothelial cells guided by Cys-Ala-Gly peptide density gradient on antifouling polymer brushes, Macromol. Biosci. 19 (2019), 1900292.
[16] M. Khan, J. Yang, C. Shi, J. Lv, Y. Feng, W. Zhang, Surface tailoring for selective endothelialization and platelet inhibition via a combination of SI-ATRP and click chemistry using Cys-Ala-Gly-peptide, Acta Biomater. 20 (2015) 69–81.
[17] L. Bai, J. Zhao, Q. Li, J. Guo, X. Ren, S. Xia, W. Zhang, Y. Feng, Biofunctionalized electrospun PCL-PIBMD/SF vascular grafts with PEG and cell-adhesive peptides for endothelialization, Macromol. Biosci. 19 (2019), 1800386.
[18] B. Yi, Q. Xu, W. Liu, An overview of substrate stiffness guided cellular response and its applications in tissue regeneration, Bioact. Mater. 15 (2022) 82–102.
[19] H.G. Sundararaghavan, R.L. Saunders, D.A. Hammer, J.A. Burdick, Fiber alignment directs cell motility over chemotactic gradients, Biotechnol. Bioeng. 110 (2013) 1249–1254.
[20] E. Vatankhah, M.P. Prabhakaran, D. Semnani, S. Razavi, M. Zamani, S. Ramakrishna, Phenotypic modulation of smooth muscle cells by chemical and mechanical cues of electrospun tecophilic/gelatin nanofibers, ACS Appl. Mater. Interfaces 6 (2014) 4089–4101.
[21] Q. Sun, Y. Hou, Z. Chu, Q. Wei, Soft overcomes the hard: flexible materials adapt to cell adhesion to promote cell mechanotransduction, Bioact. Mater. 10 (2022) 397–404.
[22] B. Yi, L. Yu, H. Tang, W. Wang, W. Liu, Y. Zhang, Lysine-doped polydopamine coating enhances antithrombogenicity and endothelialization of an electrospun aligned fibrous vascular graft, Appl. Mater. Today 25 (2021), 101198.
[23] B. Yi, Y. Shen, H. Tang, X. Wang, Y. Zhang, Stiffness of the aligned fibers affects structural and functional integrity of the oriented endothelial cells, Acta Biomater. 108 (2020) 237–249.
[24] Y.M. Shin, H.J. Shin, Y. Heo, I. Jun, Y.W. Chung, K. Kim, Y.M. Lim, H. Jeon, H. Shin, Engineering an aligned endothelial monolayer on a topologically modified nanofibrous platform with a micropatterned structure produced by femtosecond laser ablation, J. Mater. Chem. B 5 (2017) 318–328.
[25] Y. Fan, Y. Zhang, Q. Zhao, Y. Xie, R. Luo, P. Yang, Y. Weng, Immobilization of nano Cu-MOFs with polydopamine coating for adaptable gasotransmitter generation and copper ion delivery on cardiovascular stents, Biomaterials 204 (2019) 36–45.
[26] J.S. Isenberg, L.A. Ridnour, E.M. Perruccio, M.G. Espey, D.A. Wink, D.D. Roberts, Thrombospondin-1 inhibits endothelial cell responses to nitric oxide in a cGMP-dependent manner, P. Natl. Acad. Sci. USA 102 (2005) 13141–13146.
[27] X. Li, F. Shen, K. Wang, S. Lin, L. Zhou, S. Chen, J. Wang, N. Huang, Endothelial mimetic multifunctional surfaces fabricated via polydopamine mediated copper immobilization, J. Mater. Chem. B 6 (2018) 7582–7593.
[28] L. Zhou, X. Li, K. Wang, F. Shen, L. Zhang, P. Li, T. Shang, J. Wang, N. Huang, Cu-II-loaded polydopamine coatings with in situ nitric oxide generation function for improved hemocompatibility, Regen. Biomater. 7 (2020) 153–160.
[29] A.B. Seabra, G.Z. Justo, P.S. Haddad, State of the art, challenges and perspectives in the design of nitric oxide-releasing polymeric nanomaterials for biomedical applications, Biotechnol. Adv. 33 (2015) 1370–1379.
[30] M.C. Jen, M.C. Serrano, R. van Lith, G.A. Ameer, Polymer-based nitric oxide therapies: recent insights for biomedical applications, Adv. Funct. Mater. 22 (2012) 239–260.
[31] X. Zhang, Y. Wang, J. Liu, J. Shi, D. Mao, A.C. Midgley, X. Leng, D. Kong, Z. Wang, B. Liu, S. Wang, A metal-organic-framework incorporated vascular graft for sustained nitric oxide generation and long-term vascular patency, Chem. Eng. J. 421 (2021), 129577.
[32] H. Lee, S.M. Dellatore, W.M. Miller, P.B. Messersmith, Mussel-inspired surface chemistry for multifunctional coatings, Science 318 (2007) 426–430.
[33] M. Zhang, X. Zhang, X. He, L. Chen, Y. Zhang, A self-assembled polydopamine film on the surface of magnetic nanoparticles for specific capture of protein, Nanoscale 4 (2012) 3141–3147.
[34] Y. Yang, P. Qi, Y. Ding, M.F. Maitz, Z. Yang, Q. Tu, K. Xiong, Y. Leng, N. Huang, A biocompatible and functional adhesive amine-rich coating based on dopamine polymerization, J. Mater. Chem. B 3 (2015) 72–81.
[35] A. Greinacher, Heparin-induced thrombocytopenia, N. Engl. J. Med. 373 (2015) 252–261.
[36] D. Datta, A. Bhinge, V. Chandran, Lysine: is it worth more? Cytotechnology 36 (2001) 3–32.
[37] W.G. McClung, D.L. Clapper, S.P. Hu, J.L. Brash, Adsorption of plasminogen from human plasma to lysine-containing surfaces, J. Biomed. Mater. Res. 49 (2000) 409–414.
[38] Z. Tang, X. Liu, Y. Luan, W. Liu, Z. Wu, D. Li, H. Chen, Regulation of fibrinolytic protein adsorption on polyurethane surfaces by modification with lysine-containing copolymers, Polym. Chem. 4 (2013) 5597–5602.
[39] B. Yi, Y. Shen, H. Tang, X. Wang, B. Li, Y. Zhang, Stiffness of aligned fibers regulates the phenotypic expression of vascular smooth muscle cells, ACS Appl. Mater. Interfaces 11 (2019) 6867–6880.
[40] H. Kuang, Y. Wang, Y. Shi, W. Yao, X. He, X. Liu, X. Mo, S. Lu, P. Zhang, Construction and performance evaluation of Hep/silk-PLCL composite nanofiber small-caliber artificial blood vessel graft, Biomaterials 259 (2020), 120288.
[41] Y. Ding, Z. Yang, C.W.C. Bi, M. Yang, S.L. Xu, X. Lu, N. Huang, P. Huang, Y. Leng, Directing vascular cell selectivity and hemocompatibility on patterned platforms

featuring variable topographic geometry and size, ACS Appl. Mater. Interfaces 6 (2014) 12062–12070.
[42] M.E. Berginski, S.M. Gomez, The Focal Adhesion Analysis Server: a web tool for analyzing focal adhesion dynamics, F1000Research 2 (2013) 68.
[43] H. Tang, B. Yi, X. Wang, Y. Shen, Y. Zhang, Understanding the cellular responses based on low-density electrospun fiber networks, Mat. Sci. Eng. C-Mater. 119 (2021), 111470.
[44] Y. Liu, Y. Fang, X. Liu, X. Wang, B. Yang, Mussel-inspired modification of carbon fiber via polyethyleneimine/polydopamine co-deposition for the improved interfacial adhesion, Compos. Sci. Technol. 151 (2017) 164–173.
[45] N.G.P. Chew, S. Zhao, C. Malde, R. Wang, Superoleophobic surface modification for robust membrane distillation performance, J. Membr. Sci. 541 (2017) 162–173.
[46] H.C. Yang, K.J. Liao, H. Huang, Q.Y. Wu, L.S. Wan, Z.K. Xu, Mussel-inspired modification of a polymer membrane for ultra-high water permeability and oil-in-water emulsion separation, J. Mater. Chem. 2 (2014) 10225–10230.
[47] S. Mascharak, P.L. Benitez, A.C. Proctor, C.M. Madl, K.H. Hu, R.E. Dewi, M. J. Butte, S.C. Heilshorn, YAP-dependent mechanotransduction is required for proliferation and migration on native-like substrate topography, Biomaterials 115 (2017) 155–166.
[48] M. Peier, T. Walpen, G. Christofori, E. Battegay, R. Humar, Sprouty2 expression controls endothelial monolayer integrity and quiescence, Angiogenesis 16 (2013) 455–468.
[49] B. Zhang, Y. Qin, L. Yang, Y. Wu, N. Chen, M. Li, Y. Li, H. Wan, D. Fu, R. Luo, L. Yuan, Y. Wang, A polyphenol-network-mediated coating modulates inflammation and vascular healing on vascular stents, ACS Nano 16 (2022) 6585–6597.
[50] D. Radke, W. Jia, D. Sharma, K. Fena, G. Wang, J. Goldman, F. Zhao, Tissue engineering at the blood-contacting surface: a review of challenges and strategies in vascular graft development, Adv. Healthc. Mater. 7 (2018), 1701461.
[51] T. Liu, Y. Liu, Y. Chen, S. Liu, M.F. Maitz, X. Wang, K. Zhang, J. Wang, Y. Wang, J. Chen, N. Huang, Immobilization of heparin/poly-L-lysine nanoparticles on dopamine-coated surface to create a heparin density gradient for selective direction of platelet and vascular cells behavior, Acta Biomater. 10 (2014) 1940–1954.
[52] J. Zhao, L. Bai, X.k. Ren, J. Guo, S. Xia, W. Zhang, Y. Feng, Co-immobilization of ACH(11) antithrombotic peptide and CAG cell-adhesive peptide onto vascular grafts for improved hemocompatibility and endothelialization, Acta Biomater. 97 (2019) 344–359.
[53] Z. Yang, Q. Tu, Y. Zhu, R. Luo, X. Li, Y. Xie, M.F. Maitz, J. Wang, N. Huang, Mussel-inspired coating of polydopamine directs endothelial and smooth muscle cell fate for re-endothelialization of vascular devices, Adv. Healthc. Mater. 1 (2012) 548–559.
[54] A. Chiumiento, S. Lamponi, R. Barbucci, Role of fibrinogen conformation in platelet activation, Biomacromolecules 8 (2007) 523–531.
[55] M. Moffa, A.G. Sciancalepore, L.G. Passione, D. Pisignano, Combined nano- and micro-scale topographic cues for engineered vascular constructs by electrospinning and imprinted micro-patterns, Small 10 (2014) 2439–2450.
[56] B.D. James, J.B. Allen, Vascular endothelial cell behavior in complex mechanical microenvironments, ACS Biomater. Sci. Eng. 4 (2018) 3818–3842.
[57] A. Hasan, A. Memic, N. Annabi, M. Hossain, A. Paul, M.R. Dokmeci, F. Dehghani, A. Khademhosseini, Electrospun scaffolds for tissue engineering of vascular grafts, Acta Biomater. 10 (2014) 11–25.
[58] F. Zhang, Q. Zhang, X. Li, N. Huang, X. Zhao, Z. Yang, Mussel-inspired dopamine-Cu-II coatings for sustained in situ generation of nitric oxide for prevention of stent thrombosis and restenosis, Biomaterials 194 (2019) 117–129.
[59] S. Chung, N.P. Ingle, G.A. Montero, S.H. Kim, M.W. King, Bioresorbable elastomeric vascular tissue engineering scaffolds via melt spinning and electrospinning, Acta Biomater. 6 (2010) 1958–1967.
[60] A. de Mel, G. Jell, M.M. Stevens, A.M. Seifalian, Biofunctionalization of biomaterials for accelerated in situ endothelialization: a review, Biomacromolecules 9 (2008) 2969–2979.
[61] J. Chen, D. Sheng, T. Ying, H. Zhao, J. Zhang, Y. Li, H. Xu, S. Chen, MOFs-based nitric oxide therapy for tendon regeneration, Nano-Micro Lett. 13 (2021) 23.
[62] H.C. Yang, R.Z. Waldman, M.B. Wu, J. Hou, L. Chen, S.B. Darling, Z.K. Xu, Dopamine: just the right medicine for membranes, Adv. Funct. Mater. 28 (2018), 1705327.
[63] W. Cha, M.E. Meyerhoff, Catalytic generation of nitric oxide from S-nitrosothiols using immobilized organoselenium species, Biomaterials 28 (2007) 19–27.
[64] Y. Duan, S. Yu, P. Xu, X. Wang, X. Feng, Z. Mao, C. Gao, Co-immobilization of CD133 antibodies, vascular endothelial growth factors, and REDV peptide promotes capture, proliferation, and differentiation of endothelial progenitor cells, Acta Biomater. 96 (2019) 137–148.
[65] T.Y. Kang, J.H. Lee, B.J. Kim, J.A. Kang, J.M. Hong, B.S. Kim, H.J. Cha, J.W. Rhie, D.W. Cho, In vivo endothelization of tubular vascular grafts through in situ recruitment of endothelial and endothelial progenitor cells by RGD-fused mussel adhesive proteins, Biofabrication 7 (2015), 015007.
[66] Z. Xing, S. Wu, C. Zhao, Y. Bai, D. Jin, M. Yin, H. Liu, Y. Fan, Vascular transplantation with dual-biofunctional ePTFE vascular grafts in a porcine model, J. Mater. Chem. B 9 (2021) 7409–7422.
[67] T.Y. Kang, J.M. Hong, B.J. Kim, H.J. Cha, D.W. Cho, Enhanced endothelialization for developing artificial vascular networks with a natural vessel mimicking the luminal surface in scaffolds, Acta Biomater. 9 (2013) 4716–4725.
[68] C. Chaabane, F. Otsuka, R. Virmani, M.L. Bochaton-Piallat, Biological responses in stented arteries, Cardiovasc. Res. 99 (2013) 353–363.
[69] L. Geddes, E. Themistou, J.F. Burrows, F.J. Buchanan, L. Carson, Evaluation of the in vitro cytotoxicity and modulation of the inflammatory response by the bioresorbable polymers poly(D,L-lactide-co-glycolide) and poly(L-lactide-co-glycolide), Acta Biomater. 134 (2021) 261–275.
[70] B. Gao, X. Wang, M. Wang, K. You, G.S.A. Suleiman, X.K. Ren, J. Guo, S. Xia, W. Zhang, Y. Feng, Superlow dosage of intrinsically bioactive zinc metal-organic frameworks to modulate endothelial cell morphogenesis and significantly rescue ischemic disease, ACS Nano 16 (2022) 1395–1408.
[71] P.K. Givissis, S.I. Stavridis, P.J. Papagelopoulos, P.D. Antonarakos, A. G. Christodoulou, Delayed foreign-body reaction to absorbable implants in metacarpal fracture treatment, Clin. Orthop. Relat. Res. 468 (2010) 3377–3383.